ORIGINAL RESEARCH

Heart-Specific Knockout of the Mitochondrial Thioredoxin Reductase (*Txnrd2*) Induces Metabolic and Contractile Dysfunction in the Aging Myocardium

Claudia Kiermayer, PhD; Emily Northrup, DVM; Anja Schrewe, PhD; Axel Walch, MD; Martin Hrabe de Angelis, PhD; Frank Schoensiegel, PhD; Hans Zischka, PhD; Cornelia Prehn, PhD; Jerzy Adamski, PhD; Raffi Bekeredjian, MD; Boris Ivandic, MD; Christian Kupatt, MD; Markus Brielmeier, DVM

***Background*—**Ubiquitous deletion of thioredoxin reductase 2 (*Txnrd2*) in mice is embryonically lethal and associated with abnormal heart development, while constitutive, heart-specific *Txnrd2* inactivation leads to dilated cardiomyopathy and perinatal death. The significance of *Txnrd2* in aging cardiomyocytes, however, has not yet been examined.

***Methods and Results*—**The tamoxifen-inducible heart-specific α*MHC-MerCreMer* transgene was used to inactivate *lox*P-flanked *Txnrd2* alleles in adult mice. Hearts and isolated mitochondria from aged knockout mice were morphologically and functionally analyzed. Echocardiography revealed a significant increase in left ventricular end-systolic diameters in knockouts. Fractional shortening and ejection fraction were decreased compared with controls. Ultrastructural analysis of cardiomyocytes of aged mice showed mitochondrial degeneration and accumulation of autophagic bodies. A dysregulated autophagic activity was supported by higher levels of lysosome-associated membrane protein 1 (LAMP1), microtubule-associated protein 1A/1B-light chain 3-I (LC3-I), and *p62* in knockout hearts. Isolated *Txnrd2*-deficient mitochondria used less oxygen and tended to produce more reactive oxygen species. Chronic hypoxia inducible factor 1, α subunit stabilization and altered transcriptional and metabolic signatures indicated that energy metabolism is deregulated.

***Conclusions*—**These results imply a novel role of *Txnrd2* in sustaining heart function during aging and suggest that *Txnrd2* may be a modifier of heart failure. **(*J Am Heart Assoc*. 2015;4:e002153 doi: 10.1161/JAHA.115.002153)**

Key Words: aging • heart failure • thioredoxin reductase 2

Heart disease remains a leading cause of disability and mortality,[1,2] not in the least due to today's aging population with its inherently heightened risk of heart failure.[3]

From the Research Unit Comparative Medicine (C. Kiermayer, E.N., M.B.), Institute of Experimental Genetics (A.S., M.H.A.), Institute of Molecular Toxicology and Pharmacology (H.Z.), Reserach Unit Analytical Pathology (A.W.), Institute of Experimental Genetics, Genome Analysis Center (C.P., J.A.), Helmholtz Zentrum München, German Research Center for Environmental Health, Neuherberg, Germany; Department of Internal Medicine III, University of Heidelberg, Heidelberg, Germany (F.S., R.B., B.I.); I. Medizinische Klinik und Poliklinik, Klinikum Rechts der Isar, TU Munich, and German Center for Cardiovascular Research (DZHK) partner site Munich Heart Alliance, Munich, Germany (C. Kupatt); Chair of Experimental Genetics, Technische Universität München, Munich, Germany (M.H.A., J.A.).

Correspondence to: Claudia Kiermayer, PhD, Helmholtz Zentrum München, German Research Center for Environmental Health, Ingolstädter Landstr 1, 85764 Neuherberg, Germany. E-mail: claudia.kiermayer@helmholtz-muenchen.de

Received April 30, 2015; accepted May 19, 2015.

Mitochondrial dysfunction and perturbations of cardiac energy metabolism are recognized as contributors in heart failure of humans and animal models.[4–7] Mitochondria are cellular high-energy compounds and a major source of reactive oxygen species (ROS), which modulate the activity of diverse redox-sensitive signaling pathways. Importantly, several mitochondrially localized antioxidant systems maintain the intracellular redox balance.[8] Of these, the thioredoxin system, consisting of thioredoxin and thioredoxin reductase (TXNRD), is capable of reducing various disulfides and participates in different cellular processes,such as proliferation or cell death, via redox-controlled signaling.[9] The incorporation of the trace element selenium as selenocystein at the C-terminal redox active site is required for the catalytic activity of TXNRDs.[10] In livestock, selenium deficiency may cause white muscle disease, a myodegenerative disease affecting skeletal and cardiac muscle. Consistently, in humans, selenium deficiency is associated with cardiomyopathies, such as Keshan disease.[11]

Txnrd2 is essential for mouse embryogenesis; its ubiquitouse deletion is associated with malformation of the embryonic heart. Cardiomyocyte-specific ablation of *Txnrd2*

resulted in perinatal death with clinical features of congestive heart failure precluding studies in adult mice.[12] Inducible deletion of *Txnrd2* revealed an increased vulnerability of the left ventricle to ischemia–reperfusion injury (eg, larger infarct size and excess loss of function), which was amenable to treatment with ROS scavengers.[13]

Thus, malfunction of *Txnrd2* not only severely affects the developing heart but also causes an increased sensitivity toward acute heart stress. Such situations, however, may be considered extreme in their high-energy demand. They do not reflect the importance of a continuously intact mitochondrial thioredoxin system in the heart. This issue, however, is of high importance with respect to identifying key factors that determine heart well-being or failure in an aging population.

We therefore investigated *Txnrd2* function in the aging heart and demonstrate that *Txnrd2* is crucial for maintaining mitochondrial integrity and normal heart function during aging.

Methods

Transgenic Mice

Mice carrying *lox*P-flanked *Txnrd2* alleles (*Txnrd2*$^{fl/fl}$) were mated to heterozygous *Txnrd2*$^{+/-}$ mice carrying a cardiomyocyte-specific *MerCreMer* transgene.[14] Generation and genotyping of *lox*P-flanked, heterozygous, and heart-specific knockout (KO) *Txnrd2* mice were described previously.[12,15]

Tamoxifen was administrated orally as described.[15] In short, tamoxifen citrate salt (10051; Chemische Fabrik Berg GmbH) and sucrose at a final concentration of 3.6 g/kg and 5%, respectively, were added to a pelleted soy-free, low-phytoestrogen diet (ssniff M-Z Phytoestrogenarm, Ssniff Spezialdiäten GmbH). Tamoxifencontaining chow was fed ad libitum for 5 weeks starting at week 6. Before and after this period, animals were fed the standard mouse diet. Mice were bred and kept at the animal facilities of the Helmholtz Zentrum München in Type II Macrolon cages with wood shavings (Altromin) as bedding at a temperature of 20°C to 24°C and a 12/12-hour light/dark cycle. Mice had free access to a standardized mouse diet (1314, Altromin) and drinking water. All animal experiments were performed in compliance with the German animal welfare law and have been approved by the institutional animal care and use committee and by the District Government of Upper Bavaria.

Echocardiography

Functional heart assays have been performed in the cardiovascular module of the German Mouse Clinic (http://www.mouseclinic.de/).[16] Left ventricular (LV) function was determined with transthoracic echocardiography by using high-frequency ultrasound biomicroscopy with a 30-MHz transducer and 30-Hz frame rate (Vevo 660; VisualSonics). Shaved and anesthetized mice (1% isoflurane; Baxter) were fixed in supine position on a heated platform with ECG electrodes attached to monitor heart rate. Body temperature was 36°C to 38°C, monitored via use of a rectal thermometer (Indus Instruments). LV parasternal short-axis views were imaged in M-mode at the papillary muscle level. Measurements from 3 cardiac cycles each of 2 recordings were averaged for LV end-diastolic internal diameter (LVEDD) and LV end-systolic internal diameter (LVESD) by using the leading-edge convention, as suggested by the American Society of Echocardiography.[17] Fractional shortening was calculated as FS (%)=[(LVEDD−LVESD)/LVEDD)]×100, ejection fraction as EF (%)={[7/(2.4+LVEDD)]×(LVEDD)3−[7/(2.4+LVESD)]×(LVESD)3}. The echocardiographer was blinded to genotype.

Noninvasive Determination of Blood Pressure

Blood pressure was measured in conscious mice with a noninvasive tail-cuff method by using the MC4000 Blood Pressure Analysis Systems (Hatteras Instruments Inc). Mice were restrained on a prewarmed metal platform in metal boxes. The tails were looped through a tail-cuff and fixed in a notch containing an optical path with an LED light and a photosensor. The blood pulse wave in the tail artery was detected by light extinction and transformed into a pulse amplitude signal. Pulse detection, cuff inflation, and pressure evaluation were automated by the system software. After 5 initial inflation runs for habituation, 12 measurement runs were performed for each animal in 1 session. Runs with movement artifacts were excluded. After 1 day of training, in which the animals were habituated to the apparatus and protocol, the measurements were performed on 4 consecutive days between 8:30 and 11:30 AM. For each animal, 20 to 48 measurements were pooled to obtain a mean over the 4 measurement days.

Quantitative Real-Time Polymerase Chain Reaction

Total RNA was isolated from whole heart homogenates by using peqGOLD TriFast reagent (30-2010; peqLab) and cDNA was generated by using a Reverse Transcription System kit (A3500; Promega Corp) by following the manufacturers' protocols. Quantitative real-time (RT)-polymerase chain reaction (PCR) was performed by using the 7500 Real Time PCR system (Applied Biosystem, Foster City, USA) and the Power SYBR Green PCR Master Mix (4367659, Applied Biosystems). Hearts were collected from 3 mice per genotype and time point. mRNA was isolated and analyzed independently in triplicate. The PCR (50°C for 2 minutes, denaturation at 95°C

for 10 minutes, followed by 40 cycles at 95°C for 15 seconds and 60°C for 1 minutes) was performed in triplicate and normalized to endogenous *Gapdh* mRNA levels for each reaction. Quantification was done by using the comparative method ($2^{-\Delta\Delta Ct}$) of relative quantification.[18] PCR product specificity was controlled by melting curve analysis. For quantification of *Txnrd2* mRNA levels, intron-spanning primers were designed by using Primer Express Software v2.0 (Applied Biosystems), and sequences were as follows: *Act b* F 5′-TTC CGA TGC CCT GAG GC-3′, *Act b* R 5′-TCA ACG TCA CAC TTC ATG ATG ATG G-3′; *Gapdh* E5 5′-CAA TGT GTC CGT GGA TC-3′, *Gapdh* E6 5′-CCT TCA GTG GGC CCT CAG A-3′; *Txnrd2* E16 5′GCT GGG CCT GCA CTT CCT-3′, *Txnrd2* E17 5′-CTG TCT GCA TCA CCT GTG CAT-3′; *Anp* F 5′-GGC CTT TTG GCT TCC AGG-3′, *Anp* R 5′-CCT CCA GGT GGT CTA GCA GGT-3′; *p62* F 5′-GAC AGA GCA AAT GAA AAA GAT AGC C-3′, and *p62* R 5′-AAA TGT GTC CAG TCA TCG TCT CC-3′. All other primer sequences were as reported previously.[19–22]

Description of Mouse Genes Quantified by RT-PCR

The mouse genes were *Acadl*, acyl-CoA dehydrogenase, long chain (NM_007381); *Acadm*, acyl-CoA dehydrogenase, medium-chain (NM_007382); *Acot2*, mitochondrial acyl-CoA thioesterase 2 (NM_134188); *ANP*, natriuretic peptide precursor type A (NM_008725); *Bnip3,* BCL2/adenovirus E1B interacting protein 3 (NM_009760); *BNP*, natriuretic peptide precursor type B (NM_008726); *Cd36*, fatty acid translocase (NM_007643); *Etfdh*, electron transferring flavoprotein, dehydrogenase (NM_025794); *Glut1*, *Slc2a1* solute carrier family 2 (facilitated glucose transporter), member 1 (NM_011400); *Gpx1*, glutathione peroxidase 1(NM_008160); *Hif1a,* hypoxia inducible factor 1, α subunit (NM_010431); *Ldh*, lactate dehydrogenase (NM_010699); *Pdha1*, pyruvate dehydrogenase E1 α1 (NM008810); *Pdk4*, pyruvate dehydrogenase kinase, isoenzyme 4 (NM_013743); *Ppara*, peroxisome proliferator-activated receptor α (NM_011144); *Ppargc1a*, peroxisome proliferator-activated receptor, γ, coactivator (NM_008904); *p62*, *Mus musculus* sequestosome 1 (Sqstm1) (NC_000077.6); *Sod1*, superoxide dismutase 1 (NM_011434); *Sod2*, superoxide dismutase 2 (NM_013671); *Tfam*, transcription factor A, mitochondrial (NM_009360); *Ucp2*, uncoupling protein2 (NM_011671); *Ucp3*, uncoupling protein3 (NM_009464); and *Vegfa*, vascular endothelial growth factor A (NC_000083.5).

Quantification of Mitochondrial DNA

Total cellular DNA was extracted and purified from frozen hearts by using the DNeasy Tissue kit (69504, Qiagen, Hilden, Germany). Total DNA concentration was determined with a fluorometer. Equal amounts of DNA were assayed in triplicate by RT-PCR as described above by using the primers reported previously.[19] The average threshold cycle (Ct) number values of nuclear DNA (nDNA) and mitochondrial DNA (mtDNA) were used to calculate delta delta Ct as an exponent of 2 ($2^{\Delta\Delta CT}$) with ΔCt=CtnDNA−CtmtDNA.

Preparation of Heart Proteins

For the preparation of heart homogenates, mice were killed with carbon dioxide, exsanguinated and the whole organs immediately minced and homogenized on ice in 5 volumes of ice-cold homogenization buffer (HB: 20 mmol/L HEPES, pH7.4, 250 mmol/L sucrose, 1 mmol/L EDTA, 0.1 mmol/L PMSF) by using 10 strokes in a tight fit glass/glass homogenizer. Cytosolic and mitochondrial fractions were separated as previously described.[23] Protein concentration was determined by Bradford assay.

Western Blotting

Proteins were fractionated by SDS-PAGE and transferred onto a nitrocellulose membrane (Schleicher & Schuell Bioscience). The blot was blocked (1 hour at room temperature) with TBST (Tris-buffered saline, 0.1% Tween-20) containing 5% nonfat milk and then probed with the primary antibodies, in the following dilutions: 1:500 anti-TXNRD2 (Atlas Antibodies), 1:1000 anti-TXNRD2 (clone 1C4 as described earlier[24]), 1:10 000 anti-ACTIN (Sigma), 1:5000 anti-catalase (Sigma), 1:500 anti-LC3B (Sigma), 1:2000 anti-HSP60 (BD Bioscience), 1:5000 anti-HSP25 (Biomol GmbH), 1:500 anti–hypoxia inducible factor 1, α subunit (HIF1α) (Santa Cruz Biotechnology,), and 1:1000 anti-p62/SQSTM1 (Sigma). After washing with TBST (2×15 minutes), immunodetection of the signals was performed by using horseradish peroxidase–conjugated, corresponding secondary antibodies followed by 2 additional washing steps (2×10 minutes). Finally, the signal was detected by using ECL Plus Detection Reagent (Amersham Biosciences). Protein expression was quantified by using ImageJ software (National Institutes of Health).

Histology and Immunohistochemistry

Mice were sacrificed with carbon dioxide. Hearts were immediately excised, arrested with 1M KCl, weighed, fixed in 4% paraformaldehyde for 24 hours, and embedded in paraffin. Serial 5 μm sections were stained with hematoxylin and eosin. For immunohistochemistry, heat-induced epitope retrieval with the use of 0.01 mol/L sodium citrate was applied. Primary antibody dilution for anti–lysosome-associated membrane protein 1 (LAMP1) (Santa Cruz Biotechnology) was 1:500. Five representative images of LAMP1-stained

sections were acquired from each heart of 3 animals per genotype. Number of LAMP1-positive vesicles was analyzed in all images by using Fiji software.[25] For histological examination of collagen content (cardiac fibrosis), tissue was embedded in paraffin, cut into 4- to 10-μm sections, and stained with Masson trichrome. Two blinded observers scored the level of fibrosis on a scale from 0 to 3 in 9 animals per genotype. For the detection of apoptotic nuclei, terminal deoxynucleotidyl transferase dUTP nick end labeling (TUNEL) staining was performed on paraffin sections according to the manufacturer's protocol (in situ Cell Death Detection Kit, POD; Roche Diagnostics GmbH).

Quantification of Vacuolization

For determination of the severity of vacuolization in the myocardium, horizontal hematoxylin and eosin–stained paraffin sections were analyzed by 2 operators blinded to specimen origin. Per genotype (n=10), 2 consecutive sections were graded as follows: no vacuolization (0), discrete (1) if only focal vacuoles were present, moderate (2) if multifocal vacuolization was present, and intense (3) if diffuse vacuolization was present.

Mitochondrial Respiration

Mitochondria were isolated by the use of differential centrifugation. Briefly, freshly removed hearts were minced by using a razor blade and homogenized in ice-cold isolation buffer (IB: 5 mmol/L TES, 0.3 mmol/L sucrose, 0.2 mmol/L EGTA, pH 7.2, with KOH) by using 7 strokes in a tight-fit glass/glass homogenizer. Homogenates were cleared from debris and nuclei via centrifugation (700*g*, 10 minutes, 4°C), mitochondria were pelleted (11 000*g*, 15 minutes, 4°C), washed twice (11 000*g*, 10 minutes, 4°C), and resuspended in IB. Protein concentrations were determined with Bradford assay. Quality and purity were confirmed by immunoblotting the different fractions with the use of anit-GRP78 (endoplasmic reticulum marker) and anti-VDAC1 (mitochondrial marker) antibodies. Anti-VDAC1 and anti-MnSOD Western blots verified comparable mitochondrial content in the protein fractions. O_2 consumption and functional integrity of these mitochondria were assessed with the use of respiratory measurements in a Clark-type oxygen electrode (Oxygraph; Hansatech Instruments Ltd) as described previously[26] (0.25 mg/mL in respiration buffer: 0.14 mol/L mannitol, 0.05 mol/L sucrose, 5 mol/L $MgCl_2$, 0.25 mmol/L EDTA, 0.01 mol/L phosphate, 2 mmol/L Tris-HCl, pH 7.4, at 30°C with 8 mmol/L succinate).

Transmission Electron Microscopy

The left ventricle was cut into 1-mm^2 cubes and fixed with 3% glutaraldehyde in 0.1 mol/L cacodylate. Samples were post-fixed in 1% OsO_4 (4°C, 1 hour), washed 3×, dehydrated in alcohol, and embedded in Eponate. Semithin sections were stained with toluidine blue and scored by a blinded operator. Ultrathin sections were cut on the ultramicrotome, stained with uranyl acetate followed by lead citrate, and viewed with a Zeiss EM 10 CR transmission electron microscope.

ATP and GSH Measurement

Frozen heart tissue was weighed and homogenized on liquid nitrogen in a medium containing 20 mmol/L HEPES, pH 7.4, 250 mmol/L sucrose, and 1 mmol/L EDTA. For ATP measurement, the homogenate was heated immediately for 5 minutes on 95°C, cooled down on ice for 5 minutes, and centrifuged for 2 minutes at 13 000*g* on 4°C. With 50 μL of the supernatant, an ATP assay (ATP Bioluminescence Assay Kit CLS II; Roche) was performed according to the manufacturer's instructions. For reduced glutathione (GSH) measurement, the homogenate was deproteinated by using metaphosphoric acid and assayed according to the enzymatic recycling method.[27]

ROS Assay

The production of radical species in isolated mitochondria, challenged by different chemicals, was essentially measured as described.[28] Briefly, freshly isolated mitochondria were stained for 10 minutes at 0°C with 2′,7′-dichloro-dihydro-fluorescein-diacetate (D-399; Invitrogen GmbH)[29,30] in IB. After a washing step, stained mitochondria were incubated in swelling buffer (SB: 0.2 mol/L sucrose, 10 mmol/L MOPS-Tris, 5 mmol/L succinate, 1 mmol/L H_3PO_4, 10 μmol/L EGTA, 2 μmol/L rotenone) with the diverse chemicals, and the development of radical species was followed by the fluorescence of dichloro-fluorescein[31] (Ex 485/20; Em 528/20).

Metabolite Quantification

The targeted metabolomic approach was based on electrospray ionization–liquid chromatography (LC)-mass spectrometry (MS)/MS measurements by using the Absolute*IDQ* kit p180 (BIOCRATES Life Sciences AG), allowing simultaneous quantification of 186 metabolites. Heart muscle was homogenized in phosphate buffer (3 μL/mg).[32–34] Sample handling was performed with a Hamilton Microlab STAR robot (Hamilton Bonaduz AG) and an Ultravap nitrogen evaporator (Porvair Sciences), in addition to standard laboratory equipment. MS analyses were performed with an API 4000 LC/MS/MS System (AB Sciex Deutschland GmbH) equipped with a 1200 Series HPLC (Agilent Technologies Deutschland GmbH) and an HTC PAL auto sampler (CTC Analytics) controlled with use of the software Analyst 1.5. Data

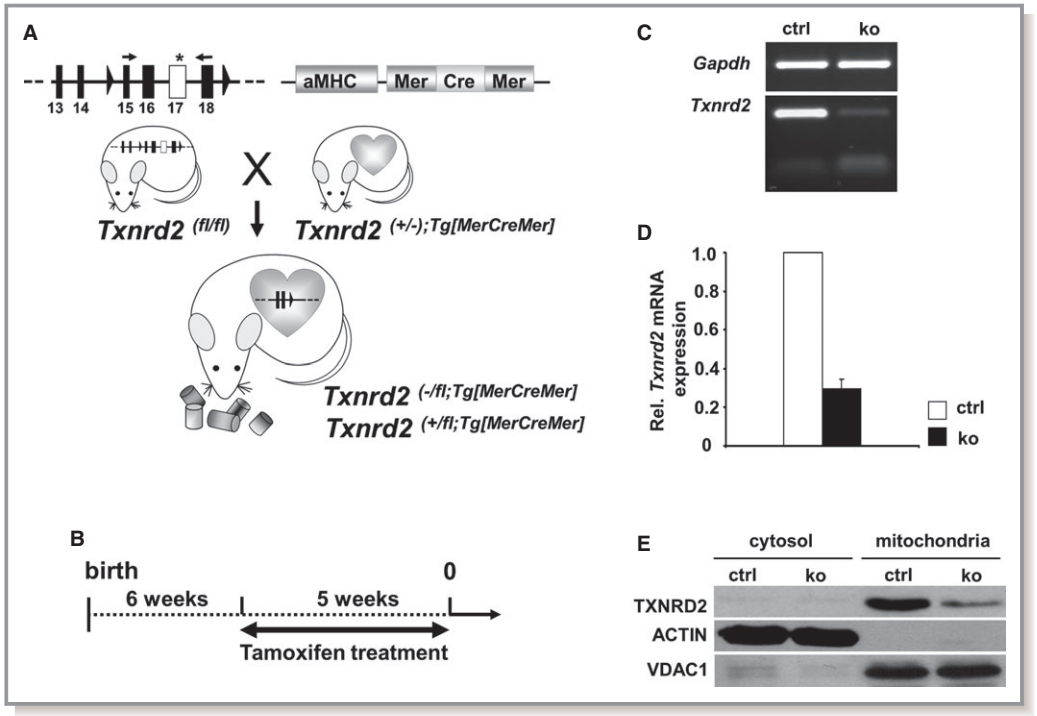

Figure 1. Reduction of cardiac *Txnrd2* expression by tamoxifen administration. A, Generation of $Txnrd2^{-/fl;Tg[MerCreMer]}$ (knockout, ko) and $Txnrd2^{+/fl;Tg[MerCreMer]}$ (control, ctrl) mice. B, To inactivate *Txnrd2*, 6-week-old ko and ctrl mice were treated with tamoxifen for 5 weeks. The end of tamoxifen treatment was defined as week 0. C, Semiquantitative RT-PCR 4 weeks after feeding tamoxifen-containing diet confirmed reduction of *Txnrd2* mRNA. D, Reduced *Txnrd2* mRNA shown by RT-PCR of whole heart cDNA. mRNA expression was normalized to *Gapdh*. Each column represents 3 independent cDNA samples (n=3). E, Reduced TXNRD2 expression in Western blot of cytosolic and mitochondrial protein fractions from whole hearts. ACTIN served as cytosolic and VDAC1 as mitochondrial loading control. αMHC indicates alpha-myosin heavy chain; RT-PCR, real-time polymerase chain reaction; TXNRD2, thioredoxin reductase 2; VDAC1, voltage-dependent anion-selective channel protein 1.

evaluation for quantification of metabolite concentrations and quality assessment were performed with the Met*IDQ* software package, which is an integral part of the Absolute*IDQ* kit. Internal standards serve as reference for the calculation of metabolite concentrations [μmol/L].

Statistical Analysis

Results are shown as mean±SD values (n=number of animals or experiments as indicated, sample sizes are given per group being compared). Comparisons between groups were performed by using the unpaired, 2-tailed Student *t* test. The paired *t* test was used when appropriate as indicated in the text. Due to small sample size (n=3), we did not apply statistical tests on quantification of mRNA- and protein-expression data. Statistical significance was defined as $P<0.05$ (*), $P<0.01$ (**), or $P<0.001$ (***).

The authors had full access to the data and take responsibility for its integrity. All authors have read and agreed to the manuscript as written.

Results

Tamoxifen-Induced Heart-Specific Knockout of *Txnrd2* in Adult Mice

Inducible heart-specific *Txnrd2*-deficient mice were generated as described.[15] Mice carrying floxed *Txnrd2* alleles ($Txnrd2^{fl/fl}$)[12] were mated to heterozygous $Txnrd^{+/-}$ mice carrying a cardiomyocyte-specific *MerCreMer* transgene.[14] The resulting $Txnrd2^{-/fl,Tg[MerCreMer]}$ mice and $Txnrd2^{+/fl,Tg[MerCreMer]}$ littermates are hereafter referred to as KOs ($Txnrd2^{-/-}$) and controls (ctrl) (Figure 1A). Animals were fed tamoxifen for 5 weeks starting at the age of 6 weeks for KO induction, and all time points reported hereafter refer to the end of tamoxifen administration (week 0) (Figure 1B). Experiments were carried out by using young (aged 5 to 6 months) (Y), middle-aged (aged 10 to 14 months) (MA), and old (aged 18 to 19 months) (O) mice as indicated. Tamoxifen administration led to a reduction in *Txnrd2* mRNA concentrations by 70±9% (n=3) and a substantial reduction in TXNRD2 protein levels in whole heart preparations of KO animals compared with controls (Figure 1C, 1D, and 1E).

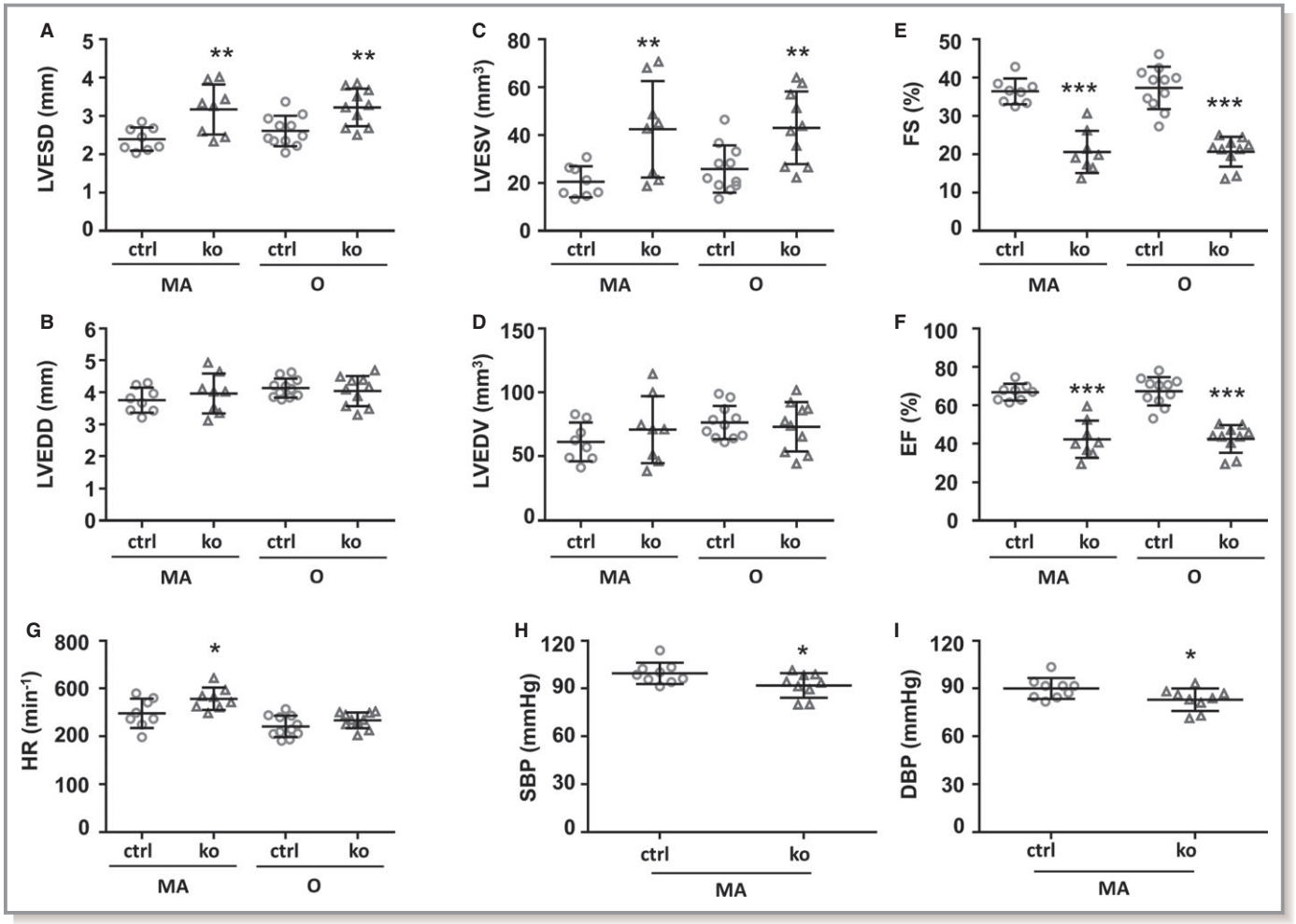

Figure 2. Impaired left ventricular function in *Txnrd2*$^{-/-}$ hearts. Results from, Echocardiography (A through G) and noninvasive measurement of blood pressure (H and I) are shown. A through G, n≥8; H and I, n=9. Time points as indicated below *x*-axis. ctrl indicates control; DBP, diastolic blood pressure; EF, ejection fraction; FS, fractional shortening; ko, knockout; LVEDD, left ventricular end-diastolic diameter; LVEDV, left ventricular end-diastolic volume; LVESD, left ventricular end-systolic diameter; LVESV, left ventricular end-systolic volume; MA, middle-aged; O, old; SBP, systolic blood pressure; *Txnrd2*, thioredoxin reductase 2.

Impaired LV Function in *Txnrd2*$^{-/-}$ Mice

Assessment of LV function by echocardiography revealed LV dysfunction in *Txnrd2*$^{-/-}$ hearts. LVESD values were significantly increased in KO animals (MA: 3.17±0.65 mm; O: 3.22±0.49 mm) compared with controls (MA: 2.39±0.3 mm; O: 2.61±0.4 mm) (MA: $P<0.01$; O: $P<0.01$) at both time points tested, whereas LVEDD values did not differ significantly (Figure 2A and 2B). Accordingly, LV end-systolic volume (LVESV) values were significantly increased in KO animals (MA: 42.40±20.13 mm^3; O: 43.01±51.19 mm^3) compared with controls (MA: 20.51±6.49 mm^3; O: 25.18±9.85 mm^3) (MA: $P<0.01$; O: $P<0.01$), whereas LV end-diastolic diameter (LVEDV) values did not differ significantly (Figure 2C and 2D).

Fractional shortening was significantly reduced in KO animals versus controls (20.58±5.50% [MA] and 20.64±3.86% [O] versus 36.40±3.35% [MA] and 37.29±5.52% [O]; MA: $P<0.001$; O: $P<0.001$) (Figure 2E). Also, LV ejection fraction was reduced significantly in KO animals versus controls (42.20±9.74% [MA] and 42.39±7.22% [O] versus 66.78±4.36% [MA] and 67.26±7.39% [O]; MA: $P<0.001$; O: $P<0.001$) (Figure 2F). Heart rate was slightly higher in KO animals versus controls (557±47 min^{-1} [MA] and 467±33 min^{-1} [O] versus 497±61 min^{-1} [MA] and 441±44 min^{-1} [O]) (Figure 2G). This increase was significant in middle-aged mice ($P<0.05$).

Reduced Blood Pressure in *Txnrd2*$^{-/-}$ Mice

Noninvasive measurements of blood pressure revealed a significant ($P<0.05$) decrease in systolic (91±7.7 mm Hg in KO versus 99.6±6.7 mm Hg in controls) and diastolic blood pressure (83.2±7.0 mm Hg in KO versus 90.1±5.6 mm Hg in controls) in KOs (Figure 2H and 2I).

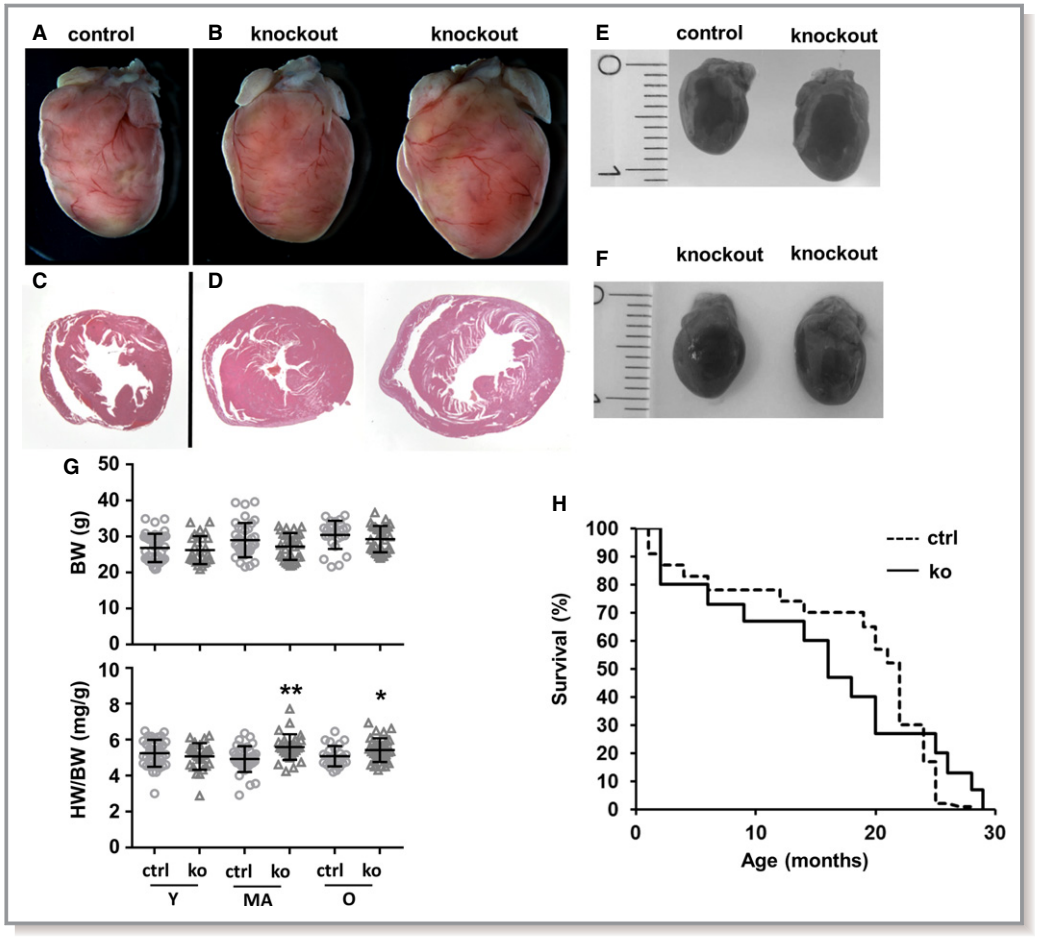

Figure 3. Gross morphological alterations in *Txnrd2*$^{-/-}$ hearts. Representative hearts of old control (A and C) and knockout mice (B and D) are shown. A and B, hearts were photographed after fixation. Appearance of *Txnrd2* knockout hearts varied, in rare cases a similar enlargement as shown in the example on the right was observed, indicating a hypertrophic response. C and D, coronary sections of the same hearts as in (A and B) were stained with H&E showing left ventricular concentric hypertrophy. Magnifications: A and B, ×6; C and D, ×8. E and F, hearts were photographed after dissection. Hearts shown in F are the same specimens as shown in (B). G, Analysis of HW and BW are shown, (G), n≥20. H, Kaplan–Meier plot showing spontaneous mortality in *Txnrd2*$^{-/-}$ mice compared with controls. Only individuals that died spontaneously after knockout induction within experimental groups are shown. Knockout and control animals were aged for the respective experiments and spontaneous mortality was recorded: 9% (15 of 164 individuals) for knockouts and 10% (23 of 219 individuals) for controls. **P*<0.05, ***P*<0.01. BW indicates body weight; H&E, hematoxylin and eosin; HW, heart weight; MA, middle-aged; O, old; *Txnrd2*, thioredoxin reductase 2; Y, young.

Gross Morphological Heart Alterations in Aged *Txnrd2*$^{-/-}$ Mice

In young mice, heart-to-body weight ratio in KOs (5.1±0.7 mg/g) was similar to that in controls (5.3±0.8 mg/g) (*P*=0.98), whereas in middle-aged mice, the heart-to-body weight ratio of KO animals was increased by ≈14% (5.6±0.7 mg/g for KO and 4.9±0.7 mg/g for controls, *P*<0.001) and by ≈6% in old mice (5.4±0.7 mg/g for KO and 5.1±0.6 mg/g for controls, *P*<0.05), indicating a mild hypertrophic response. Body weight was not altered significantly in KOs versus controls (Figure 3G). Gross morphological analysis revealed enlargement of KO hearts only in rare cases (Figure 3A versus 3B, Figure 3E and 3F). Histological analysis showed LV hypertrophy (Figure 3C versus 3D) in these *Txnrd2*$^{-/-}$ mice. Appearance, behavior, and spontaneous mortality (Figure 3H) of *Txnrd2*$^{-/-}$ mice were indistinguishable those of from age-matched controls during the observation period.

HIF1α Protein Stabilization in *Txnrd2*$^{-/-}$ Hearts

It has been shown that the mitochondrial thioredoxin system can potentially influence HIF1α protein levels.[35] Indeed, immunoblotting analysis for HIF1α detected increased protein

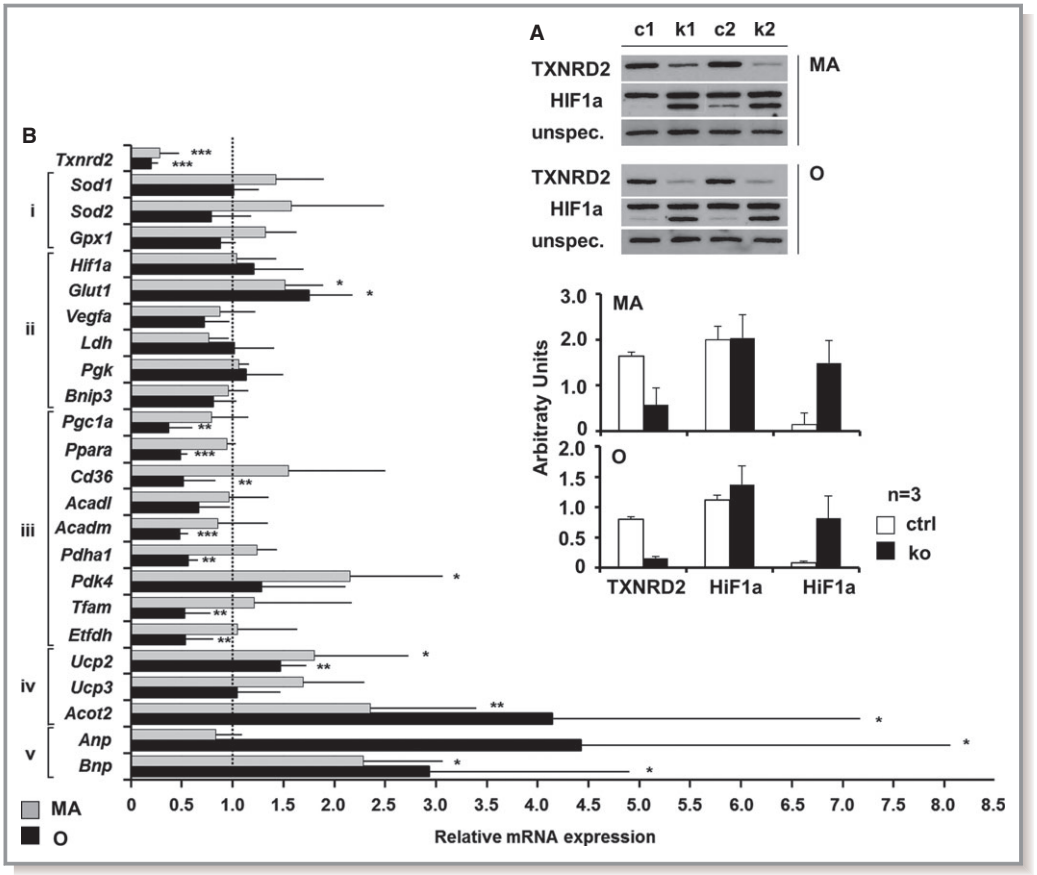

Figure 4. *Txnrd2* deletion induced HIF1a stabilization and transcriptional signature. A, Western blot (top) and quantification (bottom) showing HIF1a stabilization in knockouts, using control (c) and knockout (k) heart homogenates from MA and O mice probed with anti-TXNRD2 and anti-HIF1α antibodies. An unspecific band served as loading control. B, Alterations in relative gene expression determined by RT-PCR in *Txnrd2*$^{-/-}$ hearts of middle-aged (MA) and old (O) mice. Genes involved in oxidative stress response (i), HIF1 target genes (ii), markers for oxidative phosphorylation (iii), potential mediators of uncoupling (iv), and for LV dysfunction (v) in *Txnrd2*$^{-/-}$ hearts relative to controls. Values are the fold change in mRNA transcript level of at least 4 independent cDNA samples (n≥4) relative to control (set as 1). All probes were normalized to *Actin*. **P*<0.05, ***P*<0.01 and ****P*<0.001. LV indicates left ventricular; MA, middle-aged; O, old; RT-PCR, real-time polymerase chain reaction; *Txnrd2*, thioredoxin reductase 2.

levels of splice variant HIF1α-l.1 in KO hearts in middle-aged and old mice (≈10-fold, n=3) (Figure 4A). These data indicate an HIF1α protein stabilization, as *Hif1a* mRNA was not changed significantly (Figure 4B).

Transcriptional Signature Induced by *Txnrd2* Ablation

HIF1α target genes and markers for oxidative phosphorylation, mitochondrial biogenesis, oxidative stress response, and uncoupling proteins and for LV dysfunction were quantified by using RT-PCR (Figure 4B). While the HIF1α target genes *Vegfa* and *Bnip3* were found unchanged, *Glut-1* was induced significantly in middle-aged and old mice (MA: +52%, *P*<0.05; O: +75%, *P*<0.05). Moreover, a significant decrease was observed in fatty acid catabolism–related genes in old mice (O: *Pgc1a*, −64%, *P*<0.01; *Ppara*, −52%, *P*<0.001; *Cd36*, −49%, *P*<0.01; *Acadm*, −53%, *P*<0.001). In accordance with this, the expression of acyl-coenzyme A thioesterase 2 (*Acot2*), which typically avoids degradation of activated fatty acids by β-oxidation, was upregulated at both time points (MA: +135%, *P*<0.01; O: +314%, *P*<0.05). On the contrary, markers for glucose oxidation were differentially regulated (MA: *Pdk4*, +115; *P*<0.05; O: *Pdha1*, −45%, *P*<0.01). Importantly, genes involved in mitochondrial biogenesis and electron transfer were downregulated significantly in KO hearts from old mice (O: *Tfam*, −48%, *P*<0.01; *Pgc1a*, −64%, *P*<0.01; *Etfdh*, −48%, *P*<0.01), whereas uncoupling proteins 2 was upregulated (MA: +80% *P*<0.05; O: +46%, *P*<0.01). Hypertrophy markers (MA: *Bnp*, +128%, *P*<0.05; O: *Anp*, +324%, *P*<0.05%; *Bnp*, +193%, *P*<0.05) were strongly upregulated in *Txnrd2*$^{-/-}$ hearts at both time points (Figure 3B). Altogether, expression analysis suggests an

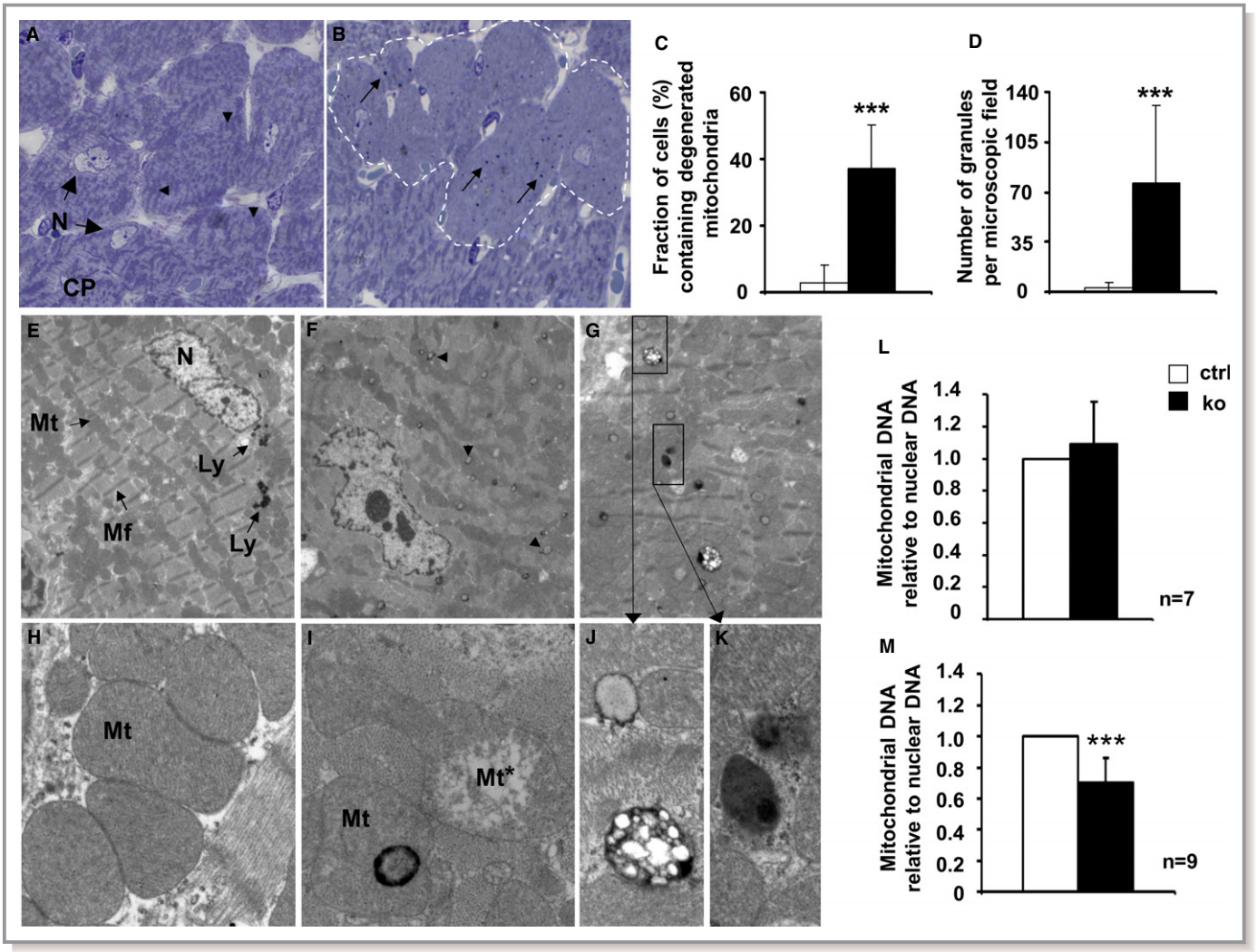

Figure 5. Presence of degenerated mitochondria in *Txnrd2*$^{-/-}$ myocardium of middle-aged mice. A, Toluidin-blue–stained semithin sections showing clearly structured mitochondria (arrowheads) in the CP of control cardiomyocytes (N=nucleus). B, Knockout hearts display myocytes with normal mitochondria alternating with myocytes containing degenerated mitochondria (broken line) and dark-stained globular structures (arrows). C, Fraction of cells containing degenerated mitochondria (n=22 [control] and n=25 [knockout] microscopic fields, 2 individuals each, total number of cells counted: 718 [controls] and 1017 [knockouts]). D, Number of granules per microscopic field in all cells (n=12 [control] and n=16 [knockout] microscopic fields, 2 individuals each). Magnification: ×100. E through K, Transmission electron micrography of the same specimens as in (A and B). E, Control myocardium shows normal myocytes containing mitochondria (Mt) of normal structure, myofibrils (Mf) and few distinct lysosomes (Ly) in the perinuclear region. F and G, knockout cardiomyocytes showing disorganized mitochondrial structures and accumulation of electron-dense and electron-light bodies (lysosome-like organelles, arrowheads). H, higher magnifications of control mitochondria. I, knockout cardiomyocytes with degenerating mitochondria (Mt*) and mitochondria containing dense bodies. Electron-light (J) and electron-dense (K) structures in close vicinity within the same cell consistent with lipofuscin accumulation. A through E, n=2 males and 2 females per genotype. Magnification: E through G, ×2520; H through K, ×20 000. L and M, mitochondrial DNA set into relation to nuclear DNA as a standard. ***P<0.001. CP indicates cytoplasm; *Txnrd2*, thioredoxin reductase 2.

altered metabolism in *Txnrd2*$^{-/-}$ hearts, specifically fatty acid metabolism. Because mitochondria are one of the major sites of FA catabolism, this indicates mitochondrial dysfunction.

Mitochondrial Degeneration in *Txnrd2*$^{-/-}$ Cardiomyocytes

Cellular alterations became obvious in toluidin blue–stained semithin sections of *Txnrd2*$^{-/-}$ myocardium in middle-aged mice. In all cardiomyocytes of control animals, mitochondria were clearly visible and formed a characteristic distribution pattern (Figure 5A, arrowheads). In contrast, in 37±13% of the KO cardiomyocytes, mitochondria and their distribution pattern were not discernible, indicating mitochondrial depletion (P<0.001, Figure 5B and 5C). In the cytoplasm of these KO myocytes, dark-blue–stained granular deposits were visible (Figure 5B, arrows). The number of these granular deposits was significantly higher in KO hearts

(76.3±54.3 for KO versus 3.3±3.5 for controls, $P<0.001$) (Figure 5D).

Transmission electron microscopy confirmed the results obtained from semithin sections. In control mice, mitochondria showed typical age-appropriate morphology and normal cytoplasmatic distribution pattern. Few distinct lysosomes were present in the perinuclear region (Figure 5E). At higher magnification, the mitochondrial matrix in controls was of homogeneous density without signs of degeneration (Figure 5H). In contrast, KO cardiomyocytes showed disorganized mitochondrial structures (Figure 5F). Ultrastructural changes included loss of cristae and matrix homogeneity (Figure 5I). Globular bodies, characterized by increased osmophilia at their periphery, were frequently associated with degenerating mitochondria (Figure 5I). The cytoplasm of KO cardiomyocytes contained numerous lysosome-like organelles showing different morphologies in size, content, and electron density (Figure 5F and 5G, arrowheads). These lysosome-like organelles exhibited electron-dense regions alternating with lucid regions, which indicated lipofuscin accumulation (Figure 5J), or a homogeneous dense matrix (Figure 5K). Signs of fibrosis, apoptosis, or inflammation were absent.

Despite mitochondrial degeneration, relative myocyte mtDNA content was not altered in KO hearts of middle-aged mice (1.09±0.26 for KO and 1.0 for controls, $P=0.36$) (Figure 5L), while it was significantly reduced in old mice by 29% (0.71±0.15 for KO and 1.0 for controls, $P<0.001$) (Figure 5M).

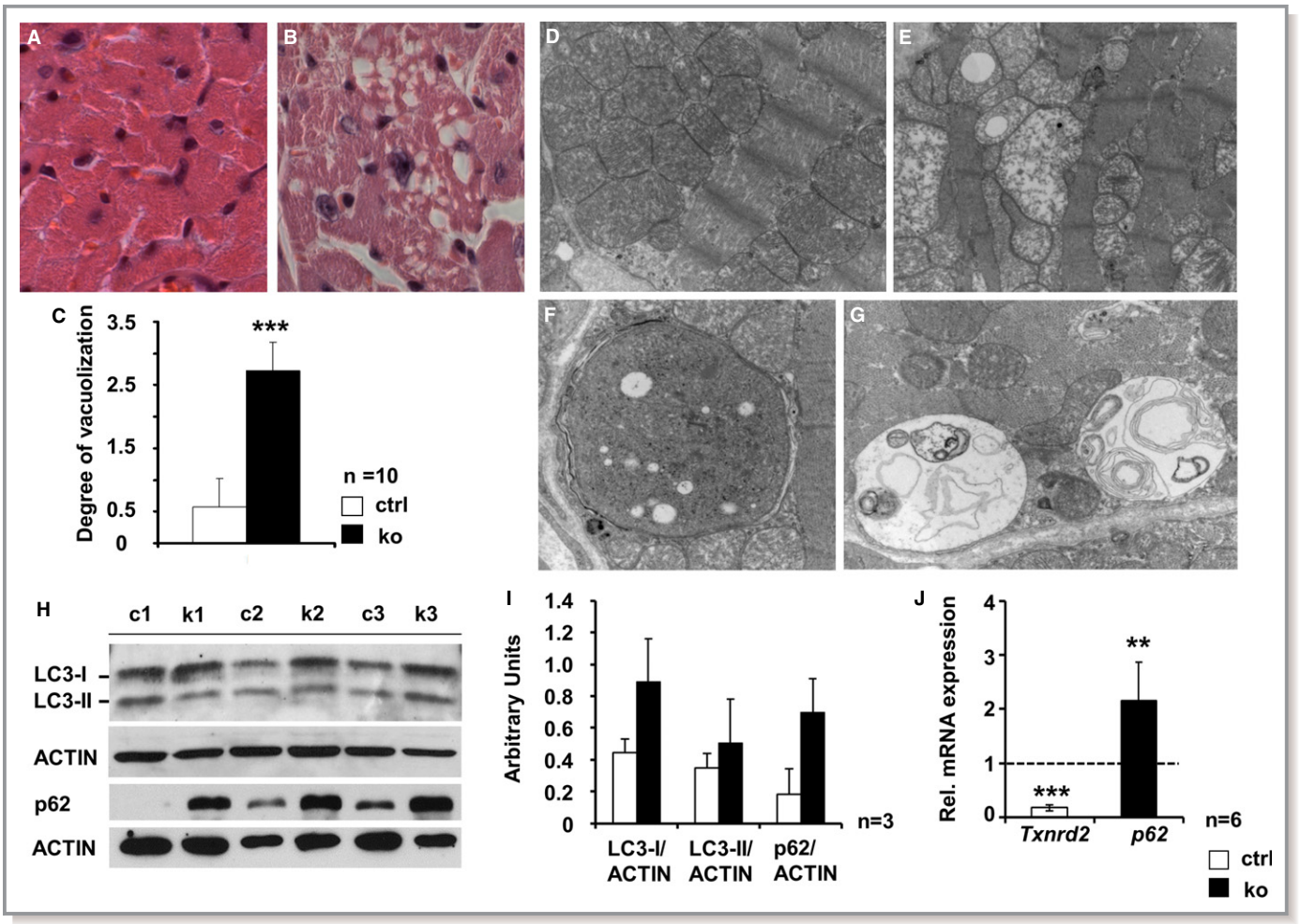

Figure 6. Autophagy in hearts of old *Txnrd2*$^{-/-}$ mice. Representative transverse sections obtained from old control (A and D), and knockout hearts (B, E, F and G). A and B, paraffin sections stained with hematoxylin and eosin. Note the markedly vacuolated cytoplasm in the knockout (B). C, quantification of vacuolization. D through G, Electron micrographs demonstrating severe mitochondrial degeneration in knockouts (E). Presence of double-membrane autophagosomes (F) and autolysosomes containing cellular material (G) in knockout cardiomyocytes (n=2). H and I, Western blots using protein homogenates obtained from 3 control (c1 to c3) and 3 knockout (k1 to k3) hearts of old mice probed with anti-LC3 and anti-p62 antibodies and corresponding quantification of protein expression. ACTIN was used as standard. J, Increased *p62* mRNA expression as analyzed by real-time RT-PCR, relative to control (set as 1). mRNA expression was normalized to *Actin*. *Txnrd2*-specific primers were used as internal control ($P<0.01$, n=6). Magnification: A and B, ×20; D and E, ×12 600; F and G, ×20 000. $^{**}P<0.01$, $^{***}P<0.001$. LC3 indicates microtubule-associated protein 1A/1B-light chain 3; RT-PCR; real-time polymerase chain reaction; *Txnrd2*, thioredoxin reductase 2.

Myocardial Degeneration and Increased Autophagic Activity in *Txnrd2*$^{-/-}$ Myocardium

Hematoxylin and eosin staining of hearts from old control mice revealed few cardiomyocytes showing cytoplasmic vacuolization. In contrast, myocardial vacuolization was 4.5-fold higher in old KO mice (2.7±0.5 for KO and 0.6±0.7 for controls, $P<0.001$) (Figure 6A through 6C). No cell infiltrates indicative of inflammation were visible. Ultrastructural analysis at the same time point confirmed the severe mitochondrial degeneration and vacuolization in KOs (Figure 6D versus 6E). Moreover, different states of autophagic degradation were present in KO cardiomyocytes, such as vacuoles sequestering dense cytoplasm (Figure 6F), designated autophagosomes, or single-membrane–bound vacuoles containing remnants of membranes and degraded cellular material (Figure 6G). Microtubule-associated protein 1A/1B-light chain 3 (LC3) is a marker of autophagic activity.[36] Western blot analysis revealed a ≈2-fold stronger 18-kDa LC3-I signal, while the LC3-II signal was not consistently increased (Figure 6H and 6I). Moreover, the protein amount of p62, being also involved in autophagosome formation,[37] was markedly upregulated in KOs (≈3.8-fold). Additionally, *p62* mRNA levels were significantly higher in KO hearts (p62: control set to 1 and 2.17±0.71 for KO, $P<0.01$) (Figure 6H through 6J). Immunostaining of lysosome-associated membrane protein 1 (LAMP1), a lysosomal marker, was significantly increased in KO hearts (Figure 7A through 7C). Masson trichrome staining showed no increase in interstitial fibrosis in young or old *Txnrd2*$^{-/-}$ mice (Figure 7D through 7F). Consistently, TUNEL staining failed to detect an increase in TUNEL-positive apoptotic nuclei in the KO myocardium (Figure 8).

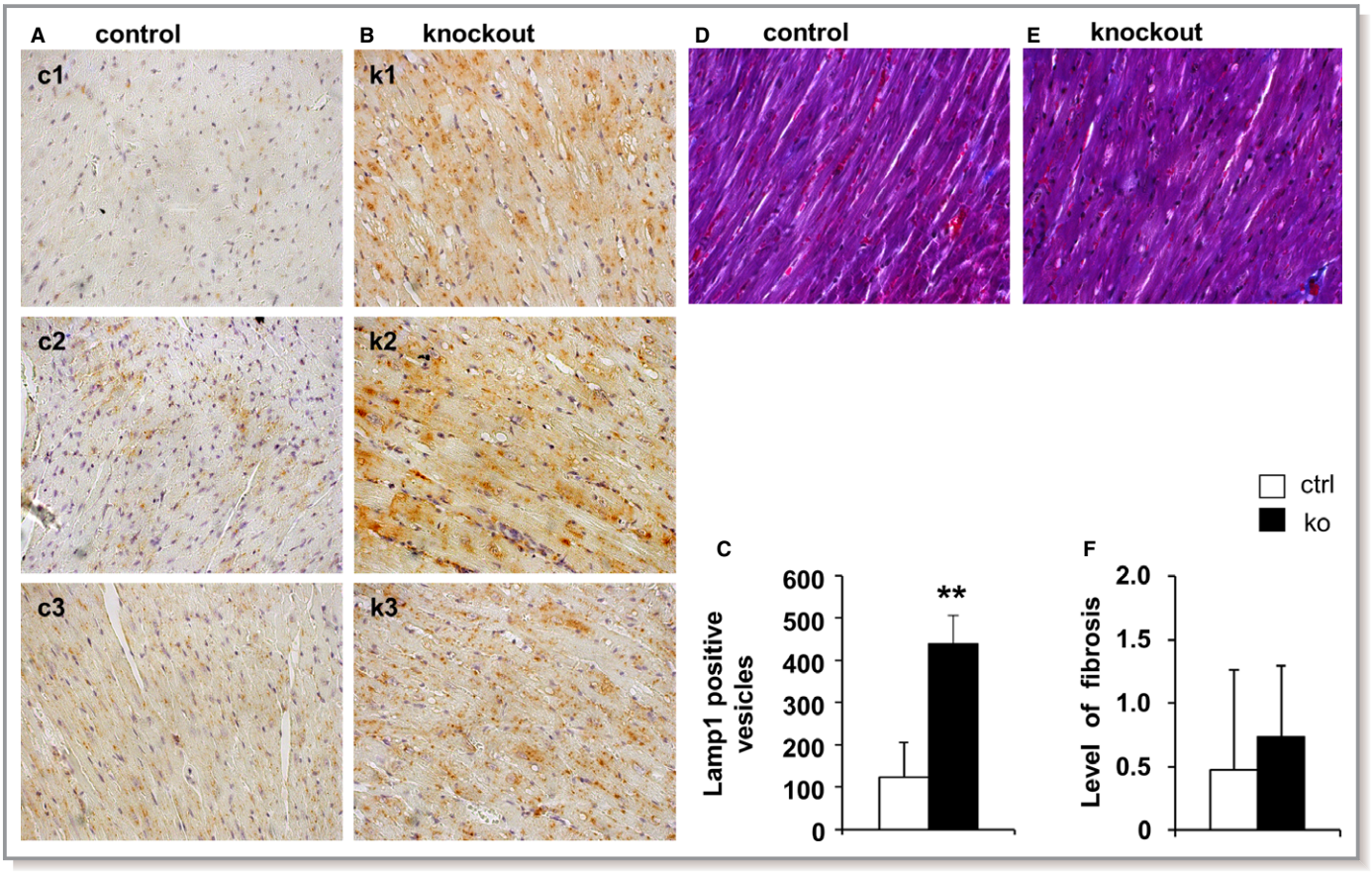

Figure 7. Increase of Lamp1 in hearts of old *Txnrd2*$^{-/-}$ mice. Representative transverse paraffin sections obtained from 3 control (c1 to c3) (A) and 3 knockout (k1 to k3) hearts (B) stained with LAMP-1 antibody, indicating enhanced lysosomal activity in knockouts. Each image represents one individual. Note the markedly vacuolated myocardium in the knockout samples (B). C, Quantification of LAMP1-positive vesicles (5 images per animal, n=3 per genotype). Magnification: A and B, ×40. D and E, Masson's Trichrome staining in *Txnrd2*$^{-/-}$ hearts. Representative transverse paraffin sections obtained from control (A) and knockout (B) hearts from old mice are shown, after Masson's Trichrome staining had been performed. No increase in collagen deposits was observed in knockout specimens compared with controls. F, Quantification of level of fibrosis, n=9 per genotype. Magnification: A and B, ×40. *$P<0.01$. LAMP1 indicates lysosomal-associated membrane protein 1; *Txnrd2*, thioredoxin reductase 2.

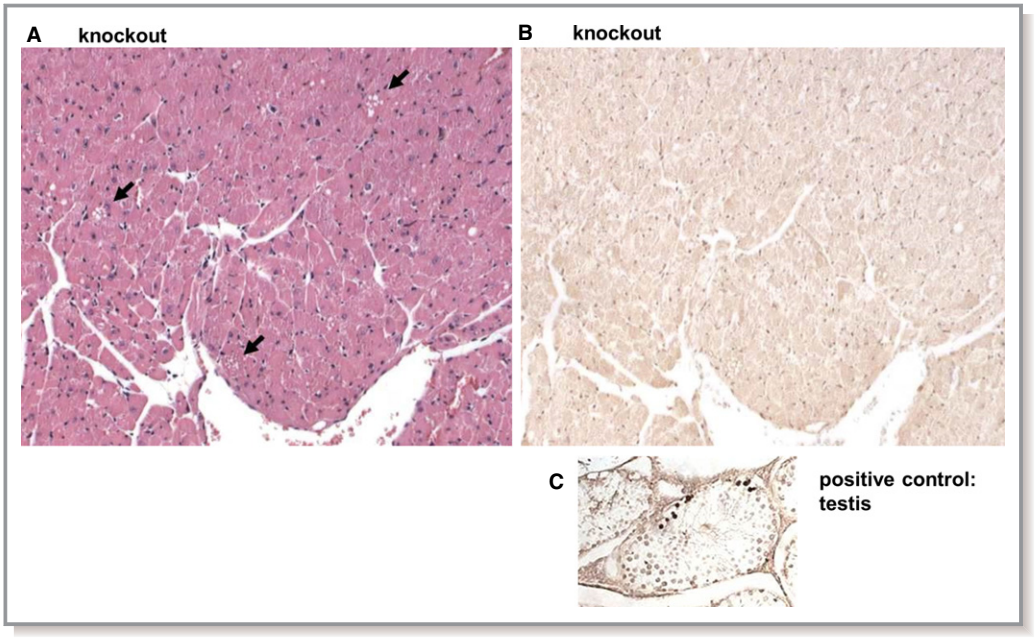

Figure 8. TUNEL staining in thioredoxin reductase 2 (*Txnrd2*$^{-/-}$) hearts. Representative transverse paraffin sections obtained from knockout hearts of old mice are shown. Sections were stained with hematoxylin and eosin (A) and consecutive sections were used for TUNEL staining (B). Throughout the myocardium vacuoles are detectable (arrows in A), in the consecutive sections no TUNEL-positive nuclei are detectable. Paraffin sections of testis were used as positive control for TUNEL staining (C). Magnification: A and B, ×20. TUNEL indicates terminal deoxynucleotidyl transferase dUTP nick end labeling.

These results indicate that autophagic activity is deregulated in aged *Txnrd2*$^{-/-}$ cardiomyocytes and emphasizes the cellular stress situation found in aged KO hearts.

Decreased Oxygen Consumption of TXNRD2-Deficient Mitochondria

Mitochondrial oxygen (O_2) consumption (Vo_2) was analyzed in isolated heart mitochondria (Figure 9A and 9B). Unaltered VDAC1 amount in these samples, as analyzed with Western blotting, demonstrated that equal amounts of mitochondria were used (data not shown). A significantly lower O_2 consumption in isolated KO compared with control mitochondria was observed at both time points applying the paired *t* test (Figure 9A and 9B, succinate-stimulated respiration [in nmol/mL per minute]: MA: 10.7±4.7 in KO versus 17.2±7.0 in controls, $P<0.05$; O: 13.5±3.4 in KO versus 18.7±5.0 in controls, $P<0.05$; ADP-stimulated respiration: MA: 22.8±9.4 in KO versus 36.3±14.6 in controls, $P=0.09$; O: 31.3±7.1 in KO versus 40.4±6.4 in controls, $P<0.01$; succinate-stimulated respiration in the presence of oligomycin and ADP: MA: 8.5±3.7 in KO versus 18.7±8.7 in controls, $P=0.09$; O: 21.4±8.5 in KO versus 26.2±8.7 in controls, $P<0.05$). Mitochondrial membrane integrity, however, as determined by the succinate-dependent respiratory control ratios was not compromised in KO mitochondria (Figure 9B, MA: 2.3±0.4 in KO versus 2.1±0.2 in controls; O: 2.7±0.7 in KO versus 2.5±0.6 in controls). This comparable mitochondrial coupling coincided with equal ATP amounts in control and KO myocardia (Figure 9C, MA: 16.5±9.2 in KO versus 18.5±17.2 in controls; O: 13.5±11.0 in KO versus 13.7±9.2 in controls). These data demonstrate that loss of *Txnrd2* impairs mitochondrial function, suggesting reduced oxidative phosphorylation.

Mitochondrial ROS Production and Induction of Antioxidative Systems

Lower O_2 consumption indicates the possibility of higher ROS production, as mitochondria produce ROS especially under decreased O_2 consumption.[38] We therefore assessed overall ROS production. In agreement, mitochondrial ROS production in old mice, measured in parallel on the same samples shown in Figure 9B by using different stressors, was increased in KO mitochondria compared with controls (Figure 10A). Although the increase in ROS production did not reach statistical significance when applying the paired *t* test, it was highly reproducible under different conditions tested. Basal ROS production of KO mitochondria incubated in isolation buffer was heightened by ≈1.27-fold (746±159 in KO versus 589±127 in controls). Challenging mitochondria by the addition of 100 μmol/L Ca^{2+}, 50 μmol/L Hg^{2+} or 100 μmol/L tertiary

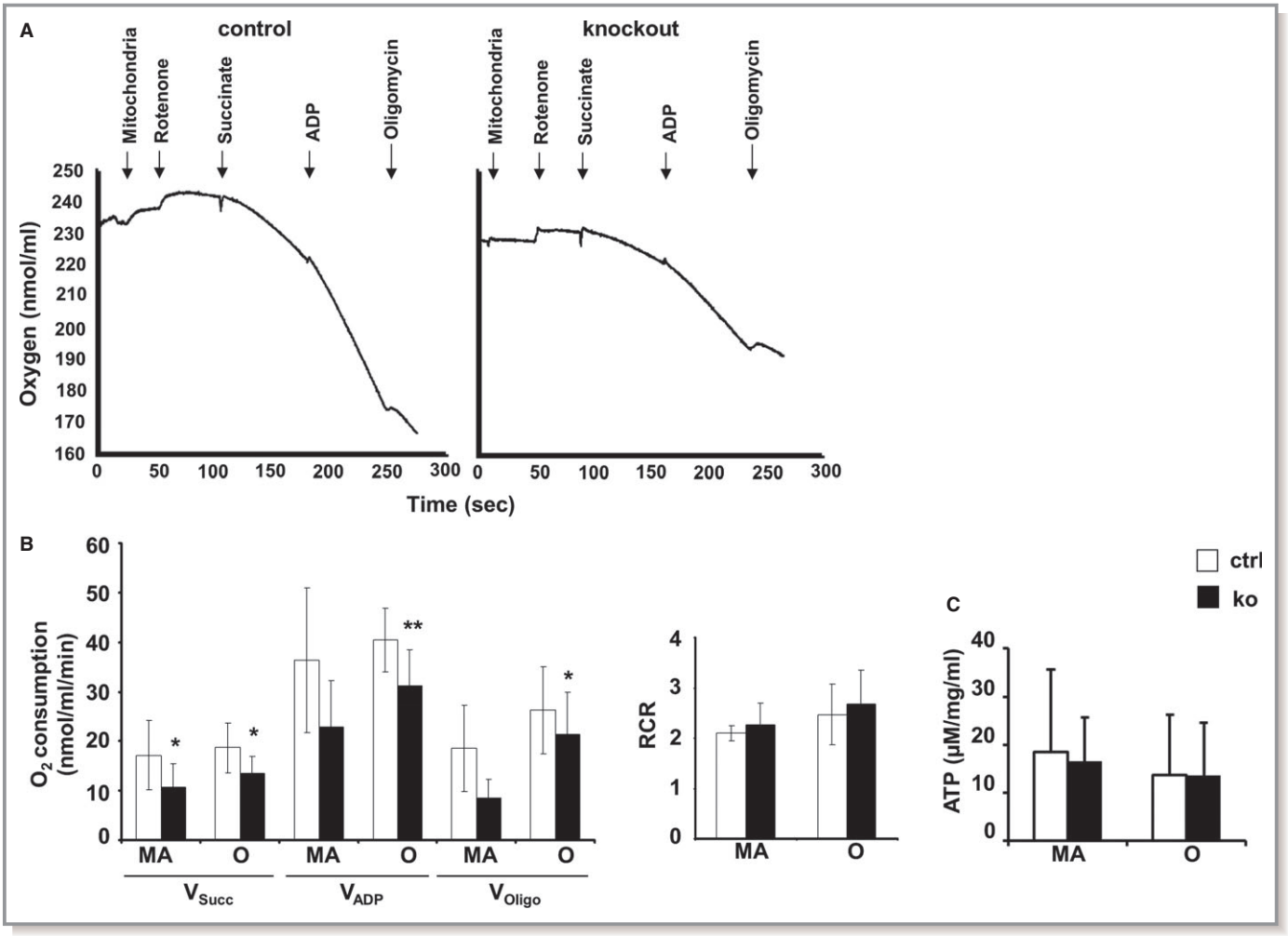

Figure 9. Membrane integrity and decreased respiration of residual mitochondria. A, Exemplary recordings of O_2 consumption by mitochondria isolated from control and knockout hearts of old mice. The graphs show 2 consecutive measurements performed at the same day. Addition of mitochondria, rotenone, succinate, ADP, and oligomycin to the assay as indicated by arrows. B, Decreased mitochondrial O_2 consumption rates (Vo_2) of mitochondria isolated from control and knockout hearts of MA (n=3) and O mice (n=7). V_{succ}: respiration in the presence of the substrate succinate (succ); V_{ADP}: respiration in the presence of succinate plus ADP; V_{Oligo}: respiration while ATP synthesis was blocked by oligomycin, an inhibitor of ATP synthase. Identical RCRs calculated as V_{ADP}:V_{succ} show membrane integrity and absence of uncoupling in MA (n=4) and O (n=7) mice. C, ATP amounts measured in myocardium from MA and O knockout mice compared with controls (n=4). **P*<0.05, ***P*<0.01. MA indicates middle-aged; O, old; RCRs, respiratory control ratios.

butylhydroperoxide (tBuOOH) did increase ROS, but the difference in ROS production between KOs and controls remained unchanged (Ca^{2+}: 802±207 in KO versus 559±127 in controls; Hg^{2+}:1323±384 in KO versus 987±353 in controls; tBuOOH: 1879±469 in KO versus 1414±474 in controls).

GSH levels (in nmol/mg protein) were significantly increased in KO myocardium at both time points (MA: 364.75±60.78 in KO versus 274.30±40.55 in controls, *P*<0.05; O: 292.33±29.93 in KO versus 227.16±26.98 in controls, *P*<0.05). As oxidized GSH (GSSG) levels were also increased, GSH/GSSG ratio was not altered (Figure 10B).

Amounts of the stress-induced proteins HSP25 and HSP60 were ≈1.6-fold higher in KO hearts from old mice. The amount of catalase protein was ≈1.9-fold greater in KOs (Figure 10C and 10D). These data support the hypothesis that increased ROS production is compensated in vivo by a cytoprotective response.

Metabolic Signature Induced by *Txnrd2* Ablation

With use of a quantitative mass spectroscopic approach, amino acids (AAs), acyl-carnitines, biogenic amines, and hexoses were measured in the myocardia of old mice (Figure 11 and Table).

Comparative analysis revealed significantly decreased levels of citrulline, histidine, and glutamine in KO myocardia. The content of all other measured AAs was increased. This change was significant with the exception of alanine, asparagine,

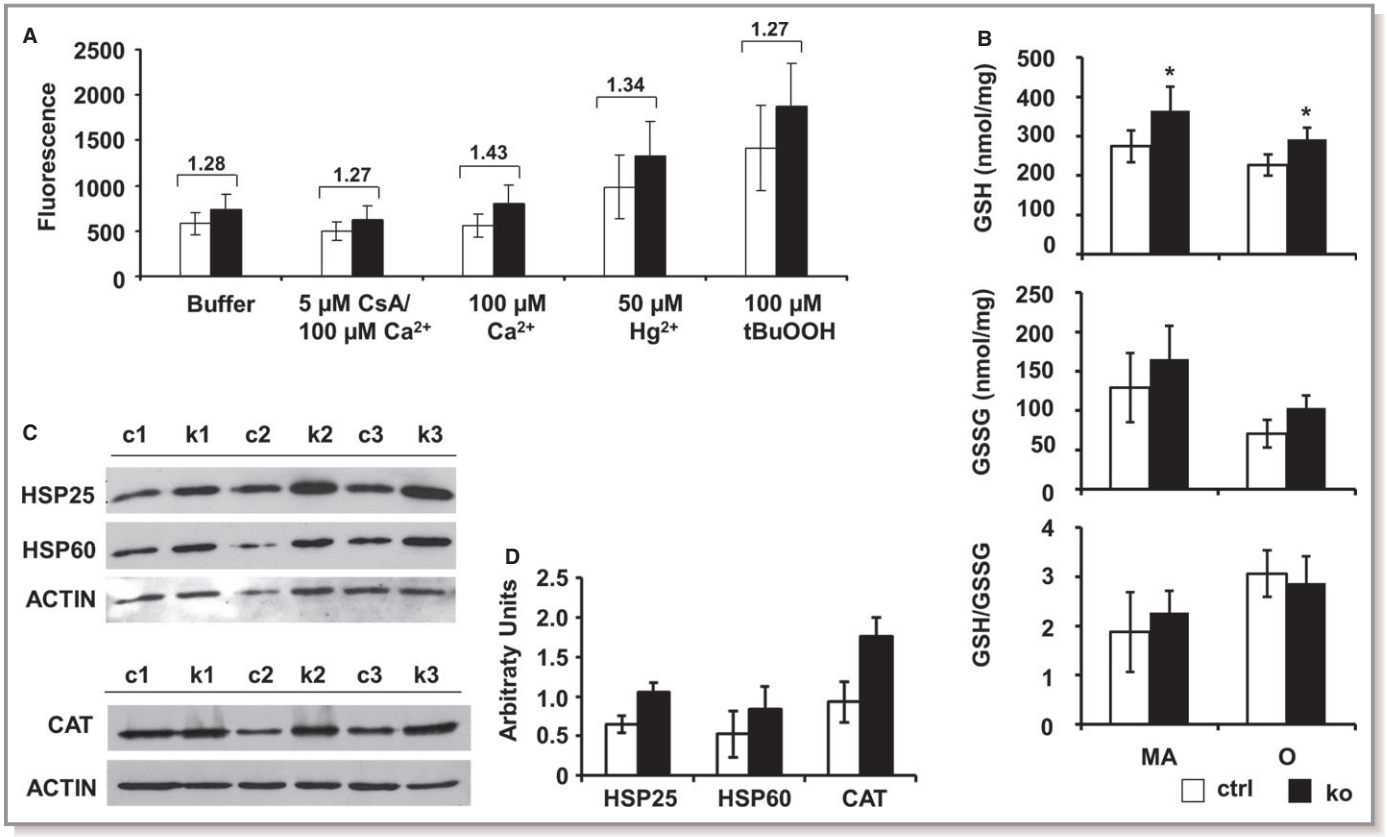

Figure 10. Increased mitochondrial ROS production in vitro and upregulation of antioxidative systems in vivo. A, Increased basal mitochondrial ROS production in knockouts measured by endpoint fluorescence after 60 minutes in vitro. Isolated mitochondria were untreated (Buffer) or stressed with 100 µmol/L calcium (Ca^{+2}), with or without CsA, 50 µmol/L mercury (Hg^{2+}) or 100 µmol/L tBuOOH (n=4). B, Amount of reduced (GSH) and oxidized glutathione (GSSG) measured in knockout myocardium from MA and O knockout mice compared with controls (n=4). C, Western blots using protein homogenates from 3 control (c1 to c3) and 3 knockout (k1 to k3) hearts probed with anti-HSP25, anti-HSP60, anti-CAT or anti-ACTIN (loading control) antibody. D, quantification indicating a stress response in knockouts. *P<0.05. CAT indicates catalase; CsA, cyclosporine A; GSH, reduced glutathione; GSSG, oxidized GSH.; MA, middle-aged; O, old; ROS, reactive oxygen species; tBuOOH, tertiary butylhydroperoxide.

phenylalanine, and tyrosine (Figure 11A). Free carnitine (C0) levels in KO hearts significantly exceeded that of control hearts by 24%, while the content of acetyl-carnitine (C2) was 25% lower in KO tissue. Among all measured acyl-carnitines the content of long-chain acyl-carnitine (C14 to C18) species was not altered. Among medium-chain acyl-carnitines (C6 to C12) the content of 2 species was significantly increased (hexenoyl-carnitine [C6.1] and pimelyl-carnitine [C7.1]), while among short-chain acyl-carnitines (C3 to C5) several were increased (malonyl-carnitine [C3.DC], butyryl-carnitine [C4], butenyl-carnitine [C4.1], and tiglyl-carnitine [C5.1]) in KO compared with control tissue (Figure 11C). From the measured biogenic amines, histamine was increased by 153% and serotonin was decreased by 49% in KO tissue (Figure 11B). Finally, the content of hexoses (90% glucose) was 36% lower in KO tissue (Figure 11D).

Quantifying metabolite concentrations provides a "snapshot" of cellular metabolism that does not reflect metabolic flux but has the potential to assign a specific phenotype.[39] Thus, the change in metabolite concentration suggests metabolic remodeling in *Txnrd2*$^{-/-}$ hearts, and again confirms the existence of cellular stress. In accordance with mitochondrial dysfunction, the altered metabolic signature of *Txnrd2*$^{-/-}$ hearts indicates a deregulation of β-oxidation and tricarboxylic acid cycle activity.

Discussion

The present study demonstrates a novel role of *Txnrd2* in the aging heart, including LV function, tissue integrity, and mitochondrial and metabolic alterations. Absence of *Txnrd2* function impairs morphological and functional integrity of mitochondria, as well as being associated with metabolic derangements and contractile dysfunction in the aging mouse heart.

Cardiac-specific ablation of *Txnrd2* was associated with a reduced LV pump function and increased LVESD in KO hearts

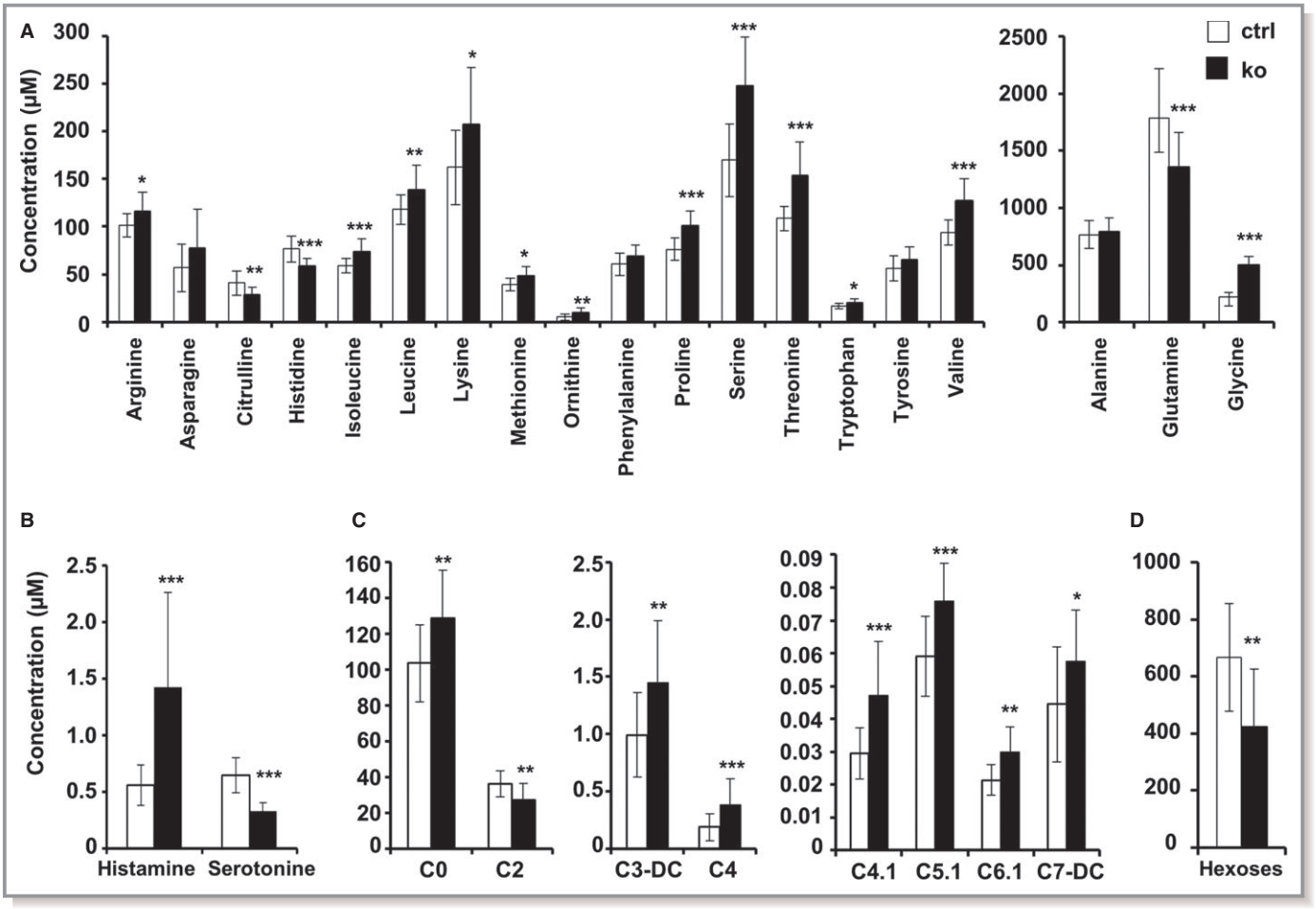

Figure 11. Alterations in metabolite levels. A through D, Concentration of selected metabolites in thioredoxin reductase 2 (*Txnrd2*$^{-/-}$) myocardium obtained from old mice compared with controls. Metabolite class A, amino acids; B, biogenic amines; C, acyl-carnitines; D, hexoses. n=14 for ko and n=15 for ctrl. *P<0.05, **P<0.01 and ***P<0.001. P-values are given in the table.

in middle-aged and old mice. Consistent with systolic dysfunction, fractional shortening and ejection fraction were reduced. The expression of natriuretic peptides, diagnostic markers of cardiovascular disease,[40] was increased.

Therefore, TXNRD2 may be critical in the progression of heart failure of patients with ischemic heart disease, genetic cardiomyopathies, or additional disorders. In accordance with this, Sibbing et al identified 3 heterozygous carriers of *Txnrd2* mutations in a cohort of 227 patients diagnosed with dilated cardiomyopathy.[41] Further, adequate selenium supply and functional selenoproteins are factors in preventing chronic heart disease.[11,42] To date, clinical trials do not support use of selenium supplements for the prevention of chronic heart disease in healthy adults.[43] However, the genetic impact of single selenoproteins is not well studied and this, along with the individuals' basic selenium intake, may have implications on selenium supplementation.

Mitochondrial degeneration observed in cardiomyocytes of aged KO mice could be a direct consequence of *Txnrd2* ablation leading to decreased energy supply, which, in turn, reduces myocardial contractility. Indeed, *Txn2* haploinsufficiency has been associated with decreased ATP production in vitro, particularly in tissues with high energy demand, such as heart.[44] Interestingly, despite obvious mitochondrial degeneration in ultrastructure, overall mitochondrial content was reduced only in old KO mice, indicating that compensatory mechanisms exist but become increasingly ineffective during aging. Consistently, *Tfam*, a gene involved in mitochondrial biogenesis, was lower in old but not in middle-aged mice.

Moreover, autophagy, a cellular process responsible for turnover of organelles and cytoplasmic proteins, is the major mitochondrial degradation pathway.[45] Autophagy is typically accompanied by accumulation of undegradable organic and anorganic material in secondary lysosomes, called lipofuscin. This age pigment was more pronounced in *Txnrd2*$^{-/-}$ hearts. Western blotting revealed an increase in the 18-kDa LC3-I signal in the myocardium of old KOs, while the LC3-II signal, representing the 16-kDa active isoform localized to autophagosome membranes and degraded during autophagy,[46]

Table. List of Acyl-carnitines, Amino Acids, Biogenic Amines, and Sugar Included in This Study

Analyte Description			Control		Knockout		*P* Value
Metabolite Class	Short Name	Biochemical Name	Mean	SD	Mean	SD	*t* Test
	Calculated total carnitine (C0 to C18)		143.83	26.740	160.99	25.590	
	Calclated total acyl-carnitines (C2 to C18)		40.06	7.631	31.81	9.145	0.01
	Acyl/free ratio		0.392	0.073	0.254	0.082	<0.001
	Summed short-chain acyl-carnitines (C3 to C5)		2.568	0.6889	3.312	0.8628	0.01
	Summed medium-chain acyl-carnitines (C6 to C12)		6.000	0.200	0.680	0.148	
	Summed long-chain acyl-carnitines (C14 to C18)		0.6502	0.3473	0.5409	0.2713	
Acyl-carnitines	C0	DL-Carnitine (free carnitine)	104	21.5	129‡	26.5	0.009
	C10	Decanoyl-L-carnitine	0.068*	0.029	0.071*	0.017	
	C10.1	Decenoyl-L-carnitine	0.067*	0.032	0.076*	0.026	
	C10.2	Decadienyl-L-carnitine	0.025*	0.013	0.031*	0.010	
	C12	Dodecanoyl-L-carnitine	0.042*	0.019	0.050*	0.019	
	C12.DC	Dodecanedioyl-L-carnitine	0.11*	0.047	0.12*	0.028	
	C12.1	Dodecenoyl-L-carnitine	0.065*	0.031	0.008*	0.026	
	C14	Tetradecanoyl-L-carnitine	0.025*	0.0075	0.023*	0.0080	
	C14.1	Tetradecenoyl-L-carnitine	0.016	0.0062	0.021	0.011	
	C14.1.OH	Hydroxytetradecenoyl-L-carnitine	0.015	0.0050	0.012*	0.0024	
	C14.2	Tetradecadienyl-L-carnitine	0.006*	0.002	0.006*	0.001	
	C14.2.OH	Hydroxytetradecadienyl-L-carnitine	0.01*	0.002	0.01*	0.001	
	C16	Hexadecanoyl-L-carnitine	0.066†	0.040	0.043†	0.028	
	C16.OH	Hydroxyhexadecanoyl-L-carnitine	0.020	0.0078	0.021	0.0097	
	C16.1	Hexadecenoyl-L-carnitine	0.052*	0.016	0.056*	0.021	
	C16.1.OH	Hydroxyhexadecenoyl-L-carnitine	0.021	0.011	0.022	0.014	
	C16.2	Hexadecadienyl-L-carnitine	0.01	0.004	0.01	0.004	
	C16.2.OH	Hydroxyhexadecadienyl-L-carnitine	0.01*	0.004	0.01*	0.003	
	C18	Octadecanoyl-L-carnitine	0.03†	0.0080	0.022†	0.012	
	C18.1	Octadecenoyl-L-carnitine	0.20	0.14	0.11	0.095	
	C18.1.OH	Hydroxyoctadecenoyl-L-carnitine	0.042	0.022	0.046	0.027	
	C18.2	Octadecadienyl-L-carnitine	0.13	0.10	0.12	0.085	
	C2	Acetyl-L-carnitine	36.2‡	7.27	27.3	9.28	0.007
	C3	Propionyl-L-carnitine	0.428	0.117	0.475	0.226	
	C3.DC, C4.OH	Malonyl-L-carnitine/hydroxybutyryl-L-carnitine	0.992	0.369	1.45	0.538	0.01
	C3.OH	Hydroxypropionyl-L-carnitine	0.033*	0.0048	0.036*	0.097	
	C3.1	Propenoyl-L-carnitine	0.009*	0.003	0.01*	0.002	
	C4	Butyryl-L-carnitine	0.188	0.0510	0.381	0.126	<0.001
	C4.1	Butenyl-L-carnitine	0.030*	0.0078	0.047	0.016	0.001
	C5	Valeryl-L-carnitine	0.14	0.040	0.14	0.030	
	C5.DC. C6.OH	Glutaryl-L-carnitine/hydroxyhexanoyl-L-carnitine	0.10	0.032	0.12	0.028	
	C5.M.DC	Methylglutaryl-L-carnitine	0.015*	0.0029	0.015	0.0021	
	C5.OH, C3.DC.M	Methylmalonyl-L-carnitine/hydroxyvaleryl-L-carnitine	0.559	0.101	0.557	0.108	
	C5.1	Tiglyl-L-carnitine	0.059	0.012	0.076	0.011	0.001

Continued

Table. Continued

Analyte Description			Control		Knockout		*P* Value
Metabolite Class	Short Name	Biochemical Name	Mean	SD	Mean	SD	*t* Test
	C5.1.DC	Glutaconyl-L-carnitine	0.013*	0.0021	0.015*	0.0030	
	C6, C4.1.DC	Fumaryl-L-carnitine/hexanoyl-L-carnitine	0.036*	0.01	0.037*	0.0069	
	C6.1	Hexenoyl-L-carnitine	0.021*	0.0046	0.030*	0.0077	0.001
	C7.DC	Pimelyl-L-carnitine	0.044	0.018	0.058	0.016	0.04
	C8	Octanoyl-L-carnitine	0.0916*	0.0101	0.0933*	0.00969	
	C8.1	Octenoyl-L-carnitine	n.d.	n.d.	n.d.	n.d.	
	C9	Nonayl-L-carnitine	0.033*	0.016	0.037*	0.014	
	Ala	Alanine	769	125	793	118	
	Arg	Arginine	101	12.1	115	20.7	0.03
	Asn	Asparagine	56.8	25.1	77.8	40.2	
Amino acids	Asp	Aspartate	n.d.	n.d.	n.d.	n.d.	
	Cit	Citrulline	40.9	12.7	29.0	7.42	0.005
	Gln	Glutamine	1783‡	436.0	1360	298.6	0.005
	Glu	Glutamate	n.d.	n.d.	n.d.	n.d.	n.d.
	Gly	Glycine	226	36.9	499	78.5	<0.001
	His	Histidine	76.6	13.8	58.2	8.81	<0.001
	Ile	Isoleucine	59.1	7.79	73.8	13.1	0.001
	Leu	Leucine	118	15.4	138	25.7	0.01
	Lys	Lysine	162	38.9	207	59.0	0.02
	Met	Methionine	39.4	6.29	47.9	10.4	0.01
	Orn	Ornithine	5.20	3.65	9.84	4.97	0.008
	Phe	Phenylalanine	60.7	11.8	68.7	12.2	
	Pro	Proline	76.3	12.0	100.	15.6	<0.001
	Ser	Serine	170.	38.1	247	51.4	<0.001
	Thr	Threonine	108	12.9	153	34.8	<0.001
	Trp	Tryptophan	16.9	2.77	20.0	4.37	0.03
	Tyr	Tyrosine	56.1	12.9	65.7	13.4	
	Val	Valine	93.5	13.0	127	23.6	<0.001
Sugar	H1	Hexose	667	189	424	202	0.002
Biogene amines	Creatinine	Creatinine	25.5	4.38	23.4	3.55	
	ADMA	Asymetric dimethylarginine	0.854	0.268	0.958	0.212	
	Ac-Orn	Acetylornithine	2.79	0.97	3.53	1.03	
	Carnosine	Carnosine	2.95	1.20	2.40	1.42	
	DOPA		0.940	0.597	0.725	0.352	
	Histamine	Histamine	0.557	0.182	1.42	0.842	0.001
	Kynurenine	Kynurenine	0.229	0.129	0.303	0.151	
	PEA	Phenylethylamine	n.d.	n.d.	n.d.	n.d.	
	Putrescine	Putrescine	1.67	0.536	1.882	0.408	
	Serotonin	Serotonin	0.654	0.157	0.323	0.081	<0.001
	Spermidine	Spermidine	19.8	3.76	22.44‡	5.19	

Continued

Table. Continued

Analyte Description			Control		Knockout		*P* Value
Metabolite Class	Short Name	Biochemical Name	Mean	SD	Mean	SD	*t* Test
	Spermine	Spermine	n.d.	n.d.	n.d.	n.d.	
	α-AAA	α-Aminoadipic acid	n.d.	n.d.	n.d.	n.d.	
	Total DMA	Total dimethylarginine	0.434†	0.152	0.502†	0.102	

The quantification range was determined by BIOCRATES and adopted from the manual: "Absolute*IDQ* p150 kit—Analytical Specifications" (BIOCRATES Life Sciences AG, Innsbruck, Austria). Total carnitine was defined as the concentration of all acyl-carnitines measured plus free carnitine. Total acyl-carnitine was defined as the concentration of all measured acyl-carnitines. The acyl/free ratio was defined as the sum of the concentration of all measured acyl-carnitines divided by the concentration of free carniti. n.d. indicates not detected. Quantification range: *Mean below LOD (limit of detection); †Mean below LLOQ (lower limit of quantification); ‡Mean below ULOQ (upper limit of quantification).

was not consistently increased. Autolysosomes are LAMP1 and LC3 positive.[47] The increase in LAMP1-positive vesicles is indicative of increased autophagic flux rather than downstream inhibition, as suppression of autophagy in upstream or downstream steps is believed to be accompanied by a decrease in autolysosomes.[48] p62 protein accumulates in authopagy-deficient cells; however, p62 can also be transcriptionally regulated during autophagy. Moreover, p62 is thought to be upregulated in response to oxidative stress.[49] As both p62 protein and *p62* mRNA were upregulated, this could be due to the active stress response in *Txnrd2*$^{-/-}$ hearts.

The slight but robustly increased ROS generation in isolated KO mitochondria seems to be compensated in vivo by a cytoprotective response, as suggested by heightened HSP25, HSP60, catalase, and GSH. Furthermore, *Txnrd2*$^{-/-}$ hearts did not accumulate peroxidized lipids on the whole cell or mitochondrial level, as assessed with anti–4-hydroxy-2-nonenal immunoblots (data not shown). There was also no evidence for increased oxidative damage to DNA and RNA as assessed with anti–8-hydroxy-2′-deoxyguanosine/8-hydroxyguanosin immunohistochemistry (data not shown). This suggests that, despite *Txnrd2* deficiency, a balance exists between mitochondrial ROS production and detoxification. Despite increased GSH levels in *Txnrd2*$^{-/-}$ hearts, the GSH/GSSG ratio was not altered, indicating that the redox balance is not disrupted.

Isolated mitochondria from aging KO mice, although lacking signs of uncoupled respiration, used significantly less oxygen, pointing toward a reduced oxidative phosphorylation. Intriguingly, the ATP content in the whole myocardium did not differ, again supporting the concept of an active compensation. Decreased O_2 consumption may be a consequence of an adaptive response resulting in reduced heart contractility, as energy supply is limited.

Mitochondria are oxygen sensors that increase ROS generation under hypoxic conditions and regulate a variety of responses, including HIF1α activation. The HIF1α stabilization in our model could not be attributed to mRNA changes. This posttranslational regulation is in agreement with the majority of findings.[50,51] Moreover, overexpression of TRX2 in hypoxic HEK cells reduced HIF1α accumulation, and this was attributed to *Trx2* influencing HIF1α protein synthesis.[35]

Long-term HIF1α stabilization in mouse heart was associated with cardiomyopathy and a metabolic shift toward higher glucose utilization during aging. Aging *Hif1-α*^{tg} mice, overexpressing HIF1α protein, spontaneously developed thicker septum walls and decreased fractional shortening.[52] Likewise, constitutively active HIF1α in adult mouse myocardium resulted in cardiomyopathy, characterized by higher heart weight and lower fractional shortening.[53]

Glut1 was the only HIF1α target gene upregulated in our model. In old *Txnrd2*$^{-/-}$ mice, the cardiac expression of enzymes providing reduction equivalents to the electron transport chain was changed. Genes involved in lipid metabolism, like *Pgc1a* and *Ppara*, were reduced. Mitochondrial uncoupling proteins 2 and 3 have been suggested not as physiological uncouplers but rather as influencing cellular metabolism and ROS production.[54,55] They were regulated toward reduced ROS production. The translational signature in *Txnrd2*$^{-/-}$ hearts supports the hypothesis of an altered metabolic homeostasis attributed to changes in HIF1α stabilization. However, a decreased mRNA content of nuclear-encoded mitochondrial genes could be contributing to this signature.

Acyl-carnitines are used as biomarkers for mitochondrial function because they are byproducts of fatty acid, glucose, and AA oxidation and their accumulation indicates deregulated β-oxidation and mitochondrial dysfunction.[56,57] In *Txnrd2*$^{-/-}$ and control hearts, the 2 major carnitines were free carnitine (≈80% and ≈72%) and acetyl-carnitine (≈17% and ≈25%, respectively).

Among acyl-carnitines, short-chain acyl-carnitines were the main species in KO and control hearts (≈73% and ≈67%), while medium- and long-chain acyl-carnities accounted for the rest of the acyl-carnitine pool at relatively equal amounts. The increased content of some short-chain (C3-DC, C4.1, C5.1) and medium-chain (C6.1, C7-DC) acyl-carnitine species further supports the concept of a deregulated flux through oxidative pathways in *Txnrd2*$^{-/-}$ myocardium.

The significant increase of nearly every AA in *Txnrd2*$^{-/-}$ hearts compared with controls suggests either that more AAs are supplied by protein catabolism, that there is a decreased protein biosynthesis, or that there is a decreased influx of AAs into the citric acid cycle. Both essential and nonessential AAs are increased, indicating protein catabolism origin. Glutamine, the most abundant AA in control and KO tissue, was significantly decreased in *Txnrd2*$^{-/-}$ hearts. Among several functions, glutamine can serve as energy source by feeding carbons via α-ketoglutarate into the tricarboxylic acid cycle. Additionally, it serves as a precursor for glutathione and could act as a remedy against redox imbalance. The significant hexose reduction in old KO hearts also points toward an increased glucose utilization.

This study identifies a critical role for *Txnrd2* in preserving the morphological and functional integrity of mitochondria in aging cardiomyocytes. Different experimental approaches clearly demonstrated cellular stress in aged KO hearts. Thus, TXNRD2 not only is important in balancing acute stress like ischemia–reperfusion but also is essential in avoiding age-related functional cardiac decline.

Acknowledgments

We thank Claudia Ludwig, Carla Fehl, and Josef Lichtmanegger for excellent technical assistance and the animal caretakers for their dedicated help. We thank Dr Werner Römisch-Margl, Julia Scarpa, and Katharina Sckell for metabolomics measurements performed at the Helmholtz Centrum München, Genome Analysis Center, Metabolomics Core Facility.

Sources of Funding

This work was mainly supported by the Priority Programme "Selenoproteins" of the German Research Foundation (DFG), grant BR 2055/1-3. Additional financial support came from grants 01GS0420 (NHK-S19T13) and 01GR0438 (PMM-S19T18) of the National Genome Research Network (NGFN) funded by the Bundesministerium für Bildung und Forschung, Germany. This study was supported in part by a grant from the German Federal Ministry of Education and Research (BMBF) to the German Center Diabetes Research (DZD e.V.).

Disclosures

None.

References

1. Go AS, Mozaffarian D, Roger VL, Benjamin EJ, Berry JD, Borden WB, Bravata DM, Dai S, Ford ES, Fox CS, Franco S, Fullerton HJ, Gillespie C, Hailpern SM, Heit JA, Howard VJ, Huffman MD, Kissela BM, Kittner SJ, Lackland DT, Lichtman JH, Lisabeth LD, Magid D, Marcus GM, Marelli A, Matchar DB, McGuire DK, Mohler ER, Moy CS, Mussolino ME, Nichol G, Paynter NP, Schreiner PJ, Sorlie PD, Stein J, Turan TN, Virani SS, Wong ND, Woo D, Turner MB; American Heart Association Statistics Committee, Stroke Statistics Subcommittee. Heart disease and stroke statistics—2013 update: a report from the American Heart Association. *Circulation*. 2013;127:e6–e245.
2. WHO. World Health Statistics. 2013.
3. Vigen R, Maddox TM, Allen LA. Aging of the United States population: impact on heart failure. *Curr Heart Fail Rep*. 2012;9:369–374.
4. Doenst T, Nguyen TD, Abel ED. Cardiac metabolism in heart failure: implications beyond ATP production. *Circ Res*. 2013;113:709–724.
5. Taegtmeyer H, Wilson CR, Razeghi P, Sharma S. Metabolic energetics and genetics in the heart. *Ann N Y Acad Sci*. 2005;1047:208–218.
6. Rosca MG, Hoppel CL. Mitochondrial dysfunction in heart failure. *Heart Fail Rev*. 2013;18:607–622.
7. Russell LK, Finck BN, Kelly DP. Mouse models of mitochondrial dysfunction and heart failure. *J Mol Cell Cardiol*. 2005;38:81–91.
8. Handy DE, Loscalzo J. Redox regulation of mitochondrial function. *Antioxid Redox Signal*. 2012;16:1323–1367.
9. Nordberg J, Arner ES. Reactive oxygen species, antioxidants, and the mammalian thioredoxin system. *Free Radic Biol Med*. 2001;31:1287–1312.
10. Labunskyy VM, Hatfield DL, Gladyshev VN. Selenoproteins: molecular pathways and physiological roles. *Physiol Rev*. 2014;94:739–777.
11. Loscalzo J. Keshan disease, selenium deficiency, and the selenoproteome. *N Engl J Med*. 2014;370:1756–1760.
12. Conrad M, Jakupoglu C, Moreno SG, Lippl S, Banjac A, Schneider M, Beck H, Hatzopoulos AK, Just U, Sinowatz F, Schmahl W, Chien KR, Wurst W, Bornkamm GW, Brielmeier M. Essential role for mitochondrial thioredoxin reductase in hematopoiesis, heart development, and heart function. *Mol Cell Biol*. 2004;24:9414–9423.
13. Horstkotte J, Perisic T, Schneider M, Lange P, Schroeder M, Kiermayer C, Hinkel R, Ziegler T, Mandal PK, David R, Schulz S, Schmitt S, Widder J, Sinowatz F, Becker BF, Bauersachs J, Naebauer M, Franz WM, Jeremias I, Brielmeier M, Zischka H, Conrad M, Kupatt C. Mitochondrial thioredoxin reductase is essential for early postischemic myocardial protection. *Circulation*. 2011;124:2892–2902.
14. Sohal DS, Nghiem M, Crackower MA, Witt SA, Kimball TR, Tymitz KM, Penninger JM, Molkentin JD. Temporally regulated and tissue-specific gene manipulations in the adult and embryonic heart using a tamoxifen-inducible Cre protein. *Circ Res*. 2001;89:20–25.
15. Kiermayer C, Conrad M, Schneider M, Schmidt J, Brielmeier M. Optimization of spatiotemporal gene inactivation in mouse heart by oral application of tamoxifen citrate. *Genesis*. 2007;45:11–16.
16. Gailus-Durner V, Fuchs H, Becker L, Bolle I, Brielmeier M, Calzada-Wack J, Elvert R, Ehrhardt N, Dalke C, Franz TJ, Grundner-Culemann E, Hammelbacher S, Holter SM, Holzlwimmer G, Horsch M, Javaheri A, Kalaydjiev SV, Klempt M, Kling E, Kunder S, Lengger C, Lisse T, Mijalski T, Naton B, Pedersen V, Prehn C, Przemeck G, Racz I, Reinhard C, Reitmeir P, Schneider I, Schrewe A, Steinkamp R, Zybill C, Adamski J, Beckers J, Behrendt H, Favor J, Graw J, Heldmaier G, Hofler H, Ivandic B, Katus H, Kirchhof P, Klingenspor M, Klopstock T, Lengeling A, Muller W, Ohl F, Ollert M, Quintanilla-Martinez L, Schmidt J, Schulz H, Wolf E, Wurst W, Zimmer A, Busch DH, de Angelis MH. Introducing the german mouse clinic: open access platform for standardized phenotyping. *Nat Methods*. 2005;2:403–404.
17. Sahn DJ, DeMaria A, Kisslo J, Weyman A. Recommendations regarding quantitation in M-mode echocardiography: results of a survey of echocardiographic measurements. *Circulation*. 1978;58:1072–1083.
18. Livak KJ, Schmittgen TD. Analysis of relative gene expression data using real-time quantitative PCR and the 2(-delta delta C(T)) method. *Methods*. 2001;25:402–408.
19. Boudina S, Sena S, Theobald H, Sheng X, Wright JJ, Hu XX, Aziz S, Johnson JI, Bugger H, Zaha VG, Abel ED. Mitochondrial energetics in the heart in obesity-related diabetes: direct evidence for increased uncoupled respiration and activation of uncoupling proteins. *Diabetes*. 2007;56:2457–2466.
20. Boudina S, Bugger H, Sena S, O'Neill BT, Zaha VG, Ilkun O, Wright JJ, Mazumder PK, Palfreyman E, Tidwell TJ, Theobald H, Khalimonchuk O, Wayment B, Sheng X, Rodnick KJ, Centini R, Chen D, Litwin SE, Weimer BE, Abel ED. Contribution of impaired myocardial insulin signaling to mitochondrial dysfunction and oxidative stress in the heart. *Circulation*. 2009;119:1272–1283.
21. Anderson J, Sandhir R, Hamilton ES, Berman NE. Impaired expression of neuroprotective molecules in the HIF-1-alpha pathway following traumatic brain injury in aged mice. *J Neurotrauma*. 2009;26:1557–1566.
22. Huang Y, Hickey RP, Yeh JL, Liu D, Dadak A, Young LH, Johnson RS, Giordano FJ. Cardiac myocyte-specific HIF-1alpha deletion alters vascularization, energy availability, calcium flux, and contractility in the normoxic heart. *FASEB J*. 2004;18:1138–1140.

23. Kiermayer C, Michalke B, Schmidt J, Brielmeier M. Effect of selenium on thioredoxin reductase activity in Txnrd1 or Txnrd2 hemizygous mice. *Biol Chem*. 2007;388:1091–1097.
24. Mandal PK, Seiler A, Perisic T, Kolle P, Banjac Canak A, Forster H, Weiss N, Kremmer E, Lieberman MW, Bannai S, Kuhlencordt P, Sato H, Bornkamm GW, Conrad M. System x(c)- and thioredoxin reductase 1 cooperatively rescue glutathione deficiency. *J Biol Chem*. 2010;285:22244–22253.
25. Schindelin J, Arganda-Carreras I, Frise E, Kaynig V, Longair M, Pietzsch T, Preibisch S, Rueden C, Saalfeld S, Schmid B, Tinevez JY, White DJ, Hartenstein V, Eliceiri K, Tomancak P, Cardona A. Fiji: an open-source platform for biological-image analysis. *Nat Methods*. 2012;9:676–682.
26. Fleischer S. Long-term storage of mitochondria to preserve energy-linked functions. *Methods Enzymol*. 1979;55:28–32.
27. Tietze F. Enzymatic method for quantitative determination of nanogram amounts of total and oxidized glutathione: applications to mammalian blood and other tissues. *Anal Biochem*. 1969;27:502–522.
28. Degli Esposti M. Assessing functional integrity of mitochondria in vitro and in vivo. *Methods Cell Biol*. 2001;65:75–96.
29. Wardman P. Fluorescent and luminescent probes for measurement of oxidative and nitrosative species in cells and tissues: progress, pitfalls, and prospects. *Free Radic Biol Med*. 2007;43:995–1022.
30. Wrona M, Patel KB, Wardman P. The roles of thiol-derived radicals in the use of 2′,7′-dichlorodihydrofluorescein as a probe for oxidative stress. *Free Radic Biol Med*. 2008;44:56–62.
31. Sokol RJ, Straka MS, Dahl R, Devereaux MW, Yerushalmi B, Gumpricht E, Elkins N, Everson G. Role of oxidant stress in the permeability transition induced in rat hepatic mitochondria by hydrophobic bile acids. *Pediatr Res*. 2001;49:519–531.
32. Zukunft S, Sorgenfrei M, Prehn C, Möller G, Adamski J. Targeted metabolomics of dried blood spot extracts. *Chromatographia*. 2013;76:1295–1305.
33. Illig T, Gieger C, Zhai G, Romisch-Margl W, Wang-Sattler R, Prehn C, Altmaier E, Kastenmuller G, Kato BS, Mewes HW, Meitinger T, de Angelis MH, Kronenberg F, Soranzo N, Wichmann HE, Spector TD, Adamski J, Suhre K. A genome-wide perspective of genetic variation in human metabolism. *Nat Genet*. 2010;42:137–141.
34. Romisch-Margl W, Prehn C, Bogumil R, Röhring C, Suhre K, Adamski J. Procedure for tissue sample preparation and metabolite extraction for high-throughput targeted metabolomics. *Metabolomics*. 2012;???:133–142.
35. Zhou J, Eleni C, Spyrou G, Brune B. The mitochondrial thioredoxin system regulates nitric oxide-induced HIF-1alpha protein. *Free Radic Biol Med*. 2008;44:91–98.
36. Zhu H, Tannous P, Johnstone JL, Kong Y, Shelton JM, Richardson JA, Le V, Levine B, Rothermel BA, Hill JA. Cardiac autophagy is a maladaptive response to hemodynamic stress. *J Clin Invest*. 2007;117:1782–1793.
37. Ikeda Y, Shirakabe A, Brady C, Zablocki D, Ohishi M, Sadoshima J. Molecular mechanisms mediating mitochondrial dynamics and mitophagy and their functional roles in the cardiovascular system. *J Mol Cell Cardiol*. 2015;78C:116–122.
38. Tahara EB, Navarete FD, Kowaltowski AJ. Tissue-, substrate-, and site-specific characteristics of mitochondrial reactive oxygen species generation. *Free Radic Biol Med*. 2009;46:1283–1297.
39. Raamsdonk LM, Teusink B, Broadhurst D, Zhang N, Hayes A, Walsh MC, Berden JA, Brindle KM, Kell DB, Rowland JJ, Westerhoff HV, van Dam K, Oliver SG. A functional genomics strategy that uses metabolome data to reveal the phenotype of silent mutations. *Nat Biotechnol*. 2001;19:45–50.
40. Kishimoto I, Tokudome T, Nakao K, Kangawa K. Natriuretic peptide system: an overview of studies using genetically engineered animal models. *FEBS J*. 2011;278:1830–1841.
41. Sibbing D, Pfeufer A, Perisic T, Mannes AM, Fritz-Wolf K, Unwin S, Sinner MF, Gieger C, Gloeckner CJ, Wichmann HE, Kremmer E, Schafer Z, Walch A, Hinterseer M, Nabauer M, Kaab S, Kastrati A, Schomig A, Meitinger T, Bornkamm GW, Conrad M, von Beckerath N. Mutations in the mitochondrial thioredoxin reductase gene TXNRD2 cause dilated cardiomyopathy. *Eur Heart J*. 2011;32:1121–1133.
42. de Lorgeril M, Salen P. Selenium and antioxidant defenses as major mediators in the development of chronic heart failure. *Heart Fail Rev*. 2006;11:13–17.
43. Rees K, Hartley L, Day C, Flowers N, Clarke A, Stranges S. Selenium supplementation for the primary prevention of cardiovascular disease. *Cochrane Database Syst Rev*. 2013;1:CD009671.
44. Perez VI, Lew CM, Cortez LA, Webb CR, Rodriguez M, Liu Y, Qi W, Li Y, Chaudhuri A, Van Remmen H, Richardson A, Ikeno Y. Thioredoxin 2 haploinsufficiency in mice results in impaired mitochondrial function and increased oxidative stress. *Free Radic Biol Med*. 2007;44:882–892.
45. Kim I, Rodriguez-Enriquez S, Lemasters JJ. Selective degradation of mitochondria by mitophagy. *Arch Biochem Biophys*. 2007;462:245–253.
46. Kabeya Y, Mizushima N, Ueno T, Yamamoto A, Kirisako T, Noda T, Kominami E, Ohsumi Y, Yoshimori T. LC3, a mammalian homologue of yeast Apg8p, is localized in autophagosome membranes after processing. *EMBO J*. 2000;19:5720–5728.
47. Yu L, McPhee CK, Zheng L, Mardones GA, Rong Y, Peng J, Mi N, Zhao Y, Liu Z, Wan F, Hailey DW, Oorschot V, Klumperman J, Baehrecke EH, Lenardo MJ. Termination of autophagy and reformation of lysosomes regulated by mTOR. *Nature*. 2010;465:942–946.
48. Mizushima N, Yoshimori T, Levine B. Methods in mammalian autophagy research. *Cell*. 2010;140:313–326.
49. Johansen T, Lamark T. Selective autophagy mediated by autophagic adapter proteins. *Autophagy*. 2011;7:279–296.
50. Taylor CT. Mitochondria and cellular oxygen sensing in the HIF pathway. *Biochem J*. 2008;409:19–26.
51. Papandreou I, Cairns RA, Fontana L, Lim AL, Denko NC. HIF-1 mediates adaptation to hypoxia by actively downregulating mitochondrial oxygen consumption. *Cell Metab*. 2006;3:187–197.
52. Holscher M, Schafer K, Krull S, Farhat K, Hesse A, Silter M, Lin Y, Pichler BJ, Thistlethwaite P, El-Armouche A, Maier LS, Katschinski DM, Zieseniss A. Unfavourable consequences of chronic cardiac HIF-1alpha stabilization. *Cardiovasc Res*. 2012;94:77–86.
53. Bekeredjian R, Walton CB, MacCannell KA, Ecker J, Kruse F, Outten JT, Sutcliffe D, Gerard RD, Bruick RK, Shohet RV. Conditional HIF-1alpha expression produces a reversible cardiomyopathy. *PLoS One*. 2010;5:e11693.
54. Toime LJ, Brand MD. Uncoupling protein-3 lowers reactive oxygen species production in isolated mitochondria. *Free Radic Biol Med*. 2010;49:606–611.
55. Bouillaud F. UCP2, not a physiologically relevant uncoupler but a glucose sparing switch impacting ROS production and glucose sensing. *Biochim Biophys Acta*. 2009;1787:377–383.
56. Sampey BP, Freemerman AJ, Zhang J, Kuan PF, Galanko JA, O'Connell TM, Ilkayeva OR, Muehlbauer MJ, Stevens RD, Newgard CB, Brauer HA, Troester MA, Makowski L. Metabolomic profiling reveals mitochondrial-derived lipid biomarkers that drive obesity-associated inflammation. *PLoS One*. 2012;7:e38812.
57. Makowski L, Noland RC, Koves TR, Xing W, Ilkayeva OR, Muehlbauer MJ, Stevens RD, Muoio DM. Metabolic profiling of PPARalpha−/− mice reveals defects in carnitine and amino acid homeostasis that are partially reversed by oral carnitine supplementation. *FASEB J*. 2009;23:586–604.